Physics – Uspekhi **53** (8) 755 – 787 (2010)

REVIEWS OF TOPICAL PROBLEMS

PACS numbers: **75.20. – g**, **75.60. – d**, **75.80. + q**

Diamagnetic (Condon) domains

V S Egorov

DOI: 10.3367/UFNe.0180.201008a.0785

Contents

Abstract. This paper is the first systematic review of experimental research on diamagnetic (aka Condon) domains that form in nonmagnetic metals at low temperatures due to the development of Landau levels. A variety of methods were used to study the domains. Muon spectroscopy studies showed such domains to be present in all metals studied, pointing to the universal nature of the phenomenon. For silver, the domain structure size as measured by Hall microsensors turned out to be an order of magnitude larger than expected. In beryllium, it was found that domains do not come to the surface but rather remain in the bulk of the crystal. The magnetostriction of beryllium during domain formation is measured. It is shown that magnetization current in a domain wall is entirely caused by the charge density gradient in the wall, due to the lattice being deformed oppositely in neighboring domains. It is observed for the first time that the de Haas–van Alphen effect exhibits hysteresis at the transition to the domain state, and this fact was used for the experimental determination of the phase diagrams for the domain states of silver and beryllium.

V S Egorov Russian Research Centre 'Kurchatov Institute'
pl. Akademika Kurchatova 1, 123182 Moscow, Russian Federation
Tel. (7-499) 196 71 06
E-mail: egorov@isssph.kiae.ru

Received 20 January 2010, revised 28 February 2010
Uspekhi Fizicheskikh Nauk **180** (8) 785 – 820 (2010)
DOI: 10.3367/UFNr.0180.201008a.0785
Translated by Yu V Morozov; edited by A Radzig

1. Introduction

The diamagnetic motion of electrons in a metal in the presence of a strong magnetic field at sufficiently low temperatures may lead under the conditions of the de Haas-van Alphen effect to specific instability and the splitting of the metallic state into two magnetic phases, i.e., diamagnetic domains or Condon domains (named after J H Condon, who was the first to predict them) [1]. This phenomenon is characterized by oppositely directed magnetization in neighboring phases (domains), which is several orders of magnitude lower than the applied external magnetic field, and by reverse magnetostriction, i.e., inverse lattice deformation in the domains. Such transition from the homogeneous metallic state to the inhomogeneously magnetized and deformed one may occur only in metallic single crystals of very high quality in a highly uniform and strong enough magnetic field at extremely low temperatures.

All the phenomena discussed in this review, viz. magnetization, magnetic domains, are due to the orbital diamagnetic motion of electrons alone and unrelated to electron spins. In addition to diamagnetic domains proper, we consider the closely related problems of the electronic contribution to metal compressibility and the Fermi level oscillations in a magnetic field.

A systematic presentation of the results of diamagnetic domain experiments is preceded by a brief discussion of the physical fundamentals of this phenomenon.

1.1 De Haas–van Alphen effect

The story of developing specific instability in metals which experience phase splitting into two oppositely magnetized phases dates to the well-known article "On the diamagnetism

of free electrons'' by Landau [2]. In an attempt to explain the origin of metal diamagnetism, Landau postulated for the first time the formation of equidistant energy levels (Landau levels). Equidistant energy levels form during electron motion along a closed orbit provided the electron lifetime τ between collisions is much greater than the period $2\pi/\omega$ of its revolution:

$$\omega\tau \gg 1\,.$$

As a result, Landau obtained a basically new quasicontinuous electron energy spectrum in the magnetic field:

$$E_n = \left(n+\frac{1}{2}\right)\hbar\omega + \frac{1}{2m}\,p_H^2\,.$$

Here, $n = 0, 1, 2, \ldots$, $\hbar$ is the Planck constant, $\omega = eH/(mc)$ is the cyclotron frequency, m is the electron mass, c is the speed of light, H is the magnetic field strength, and p_H is the electron momentum component in the magnetic field direction. It is essential that the minimal electron energy be $\hbar\omega/2$ rather than zero.

The total energy of such quantized electron gas exceeds the classical value by a quantity proportional to H^2. This results in negative magnetization linear in the magnetic field and thus explains the diamagnetism. Moreover, Landau found that if the magnetic field energy is higher than the thermal energy, namely

$$\hbar\omega \gg k_{\rm B}T \tag{1}$$

($k_{\rm B}$ is the Boltzmann constant), the energy of electron gas contains a small additional component rapidly oscillating in field and 'fast periodicity', i.e., oscillations of magnetization, occurs. In fact, he predicted a new effect. The free-electron model used by Landau placed heavy demands on magnetic field strength and uniformity practically unattainable at that time. Therefore, he doubted the possibility of experimental examination of the newly discovered effect. Nevertheless, magnetic moment oscillations in bismuth were soon revealed by de Haas and van Alphen [3] independently of Landau's work. The period of such oscillations in the dependence of the magnetic moment on the inverse magnetic field strength proved constant.

This phenomenon was later reported to occur in other metals and was called the de Haas–van Alphen (often abbreviated dHvA) effect. Oscillations were observed in high-quality single crystals at very low temperatures ($T \leqslant 4.2$ K) Their amplitude rapidly decreased to zero, even with a small rise in temperature. It turned out that oscillation periods in individual metals differed by several orders of magnitude, and many had more than one oscillation period, each depending on the orientation of the single-crystal sample with respect to **H**. Not surprisingly that the de Haas–van Alphen effect was considered for a rather long time to be directly unrelated to Landau's prediction.

The diversity of experimental results was explained only in the 1950s based on the concept of multiple forms and sizes of the Fermi surface, developed by Lifshits, Azbel', Kaganov, and Peschanskii (the LAKP theory) [4, 5]. Electron interactions with a periodic potential of the lattice result in a transformation of the free-electron sphere into a set of various surfaces, including multiply connected ones. In 1952, Onsager [6] showed for the first time that the magnetization oscillation period depends on the extremal cross section area of the Fermi surface normal to **H**. Finally, Lifshits and Kosevich [7] elaborated in 1955 a complete theory of metal magnetization (the LK theory) applicable to any metal with an arbitrary Fermi surface at unrestricted temperature. Certainly, the results of the LK theory and Landau's prediction for the free-electron model completely coincide. However, only the LK theory explained why Landau diamagnetism may be abnormally high in certain metals, ascribing it to the existence of abnormally high cyclotron frequencies in them.

Here are the main formulas. Longitudinal (parallel to the external magnetic field) magnetization is defined as

$$M = -M_1 \sin\left(\frac{2\pi F}{B}+\phi\right) + \sum_{p=2}^{\infty}(-M_p)\sin\left(\frac{2\pi pF}{B}+\phi_p\right),$$

which gives for susceptibility $\chi = \partial M/\partial B$ the following expression

$$\chi = -\chi_1 \cos\left(\frac{2\pi F}{B}+\phi\right) + \sum_{p=2}^{\infty}\chi_p\cos\left(\frac{2\pi pF}{B}+\phi_p\right).$$

Here, F is the dHvA magnetic frequency:

$$F = \frac{\hbar c A_{\rm ext}}{2\pi e} \tag{2}$$

(this is just the Onsager formula) determined by the extremal cross section area $A_{\rm ext}$ of the Fermi surface perpendicular to **H**. The contribution of high harmonics with $p \geqslant 2$ becomes essential at extra low temperatures and usually can be neglected. LK theory gives for the first-harmonic amplitude:

$$\chi_1(B, T;\, x_{\rm D},\, m^*,\, \ldots) = \frac{e^2}{4\pi^4 mc^2}\,A_{\rm ext}^2\left(\frac{2\pi}{|A''|}\right)^{1/2} \times \frac{m}{m^*}\left(\frac{\hbar c}{eB}\right)^{3/2} G_{\rm s}R(u,v)\,. \tag{3}$$

Here, m^* is the effective cyclotron mass corresponding to a given cross section, $A'' = \partial^2 A(k_z)/\partial k_z^2$ is the second derivative along the magnetic field (i.e., Fermi surface curvature determining the effective width of the extremal belt), $R(u, v)$ is the factor responsible for the decrease in the dHvA amplitude at finite temperature T and as a result of Landau level broadening due to scattering from lattice defects with the scattering time τ:

$$R(u,v) = \frac{u}{\sinh u}\exp(-v)\,,$$

where $u = 2\pi^2 k_{\rm B}T/(\hbar\omega_{\rm c})$, $v = 2\pi^2 k_{\rm B}x_{\rm D}/(\hbar\omega_{\rm c})$, $\omega_{\rm c} = eB/(m^*c)$ is the cyclotron frequency in the magnetic field B, $x_{\rm D}$ is the so-called Dingle temperature

$$x_{\rm D} \equiv T_{\rm D} = \frac{\hbar}{2\pi k_{\rm B}\tau}\,, \tag{4}$$

factor $G_{\rm s} = \cos\left[\pi g m^*/(2m)\right]$, and $g \approx 2$ takes into account electrons with the opposite spins. If there are several extremal cross sections in a given magnetic field direction, their contributions are summed up.

Measurement of magnetization oscillations is one of the main methods for investigating Fermi surfaces. Numerous studies have been carried out over the period of 10 years.

Measurements of the dHvA effect permit determining not only the dependences of the cross section area of the Fermi surface on field direction relative to the crystal orientation but also the relaxation time and a set of effective masses. All this provides abundant information about the electronic spectra of metals. Fermi surfaces of all or almost all metals (at least those for which high-quality single crystals were available) were determined. Moreover, oscillations of many other properties of metals were discovered, for which the oscillatory contribution to the energy, due to the formation of Landau levels, is responsible. Many remarkable phenomena observable at low temperatures are described in detail in the book by D Shoenberg [8].

The above formulas contain an average magnetic field acting on an electron traveling along a cyclotron (Larmor) orbit, i.e., induction B. The cyclotron radius ranges, as a rule, $10^{-3}-10^{-4}$ cm, or much larger than the mean interelectron distance $\sim 10^{-8}$ cm (naturally, with the exception of superstrong magnetic fields or, in other words, proximity to the ultraquantum limit). For this reason, orbits of electrons strongly overlap and their interaction at Landau levels is mediated not only by electrostatic forces but also through the formation of self-consistent magnetization $M(B)$ [8, 9]. When M is small, the difference between B and H is, as a rule, immaterial and the interaction may be neglected. Sometimes, however, it can be essential (see below), as in the case of *magnetic interaction* (MI) in the dHvA effect. MI results in developing a peculiar instability with the splitting of a metallic state of the sample into two oppositely magnetized phases, i.e., diamagnetic domains or Condon domains.

1.2 The nature of diamagnetic domains

The formation of diamagnetic domains is doubtless one of the most remarkable consequence of the dHvA effect. In order to better understand the nature of this phenomenon, we shall consider magnetization in a sample placed in a uniform external magnetic field **H**, where an additional oscillating energy $\tilde{\varepsilon}$ and, accordingly, oscillating magnetization $4\pi M$ are emerging. With MI in mind, it is assumed that $M = M(B)$. Let us consider for simplicity the limiting case of a sample in the form of an infinitely long cylinder oriented along the magnetic field (demagnetization factor $n = 0$). Then, for an overall energy change per unit volume of the sample, taking into account the magnetization current-induced energy $(B-H)^2/8\pi$ of the electromagnetic field, one can derive the following expression

$$\tilde{\varepsilon} + \frac{(B-H)^2}{8\pi} . \tag{5}$$

Because $\tilde{\varepsilon}$ is determined by the magnetic field B acting on electrons and because it oscillates in this field, B must vary with respect to H so that sum (5) take the minimally possible value, i.e., the derivative of expression (5) with respect to B was zero:

$$\frac{\partial\tilde{\varepsilon}}{\partial B} + \frac{B-H}{4\pi} = 0 ;$$

hence, the magnetic moment $M = -\partial\tilde{\varepsilon}/\partial B$, i.e., in the formula

$$B = H + 4\pi M$$

one has $M = M(B) = -\partial\tilde{\varepsilon}/\partial B$. The exact LK formula for $\tilde{\varepsilon}$ is well known [8] but, it being cumbersome, we confine ourselves to the simplest first-harmonic approximation for $\tilde{\varepsilon}$ (the so-called single-harmonic approximation) that is quite sufficient for understanding the nature of the phenomenon of interest, namely

$$\tilde{\varepsilon} = a\cos\varphi , \tag{6}$$

where the phase

$$\varphi = \frac{2\pi F}{B} .$$

Amplitude a is determined by different experimental conditions, and F by the Onsager formula (2). Evidently, when $a \ll 1$, the difference between B and H is negligibly small relative to the oscillation period, i.e., phase φ remains practically unaltered upon substitution $B \to H$. In this case, both the first derivative of $\tilde{\varepsilon}$ (magnetic moment M) and the second derivative of $\tilde{\varepsilon}$ (magnetic susceptibility), viz.

$$\chi_B = \frac{\partial M}{\partial B} \equiv -\frac{\partial^2\tilde{\varepsilon}}{\partial B^2} ,$$

must have the sine or cosine shape as functions of the magnetic field. The experimentally obtained differential susceptibility is defined as

$$\chi_H = \frac{\partial M}{\partial H} \approx \frac{\partial M}{\partial B} = \chi_B . \tag{7}$$

However, under certain conditions (low temperatures, high quality of the sample), amplitude a cannot, generally speaking, be regarded as small. In addition, it follows from expression (6) for the phase that

$$\frac{\partial\varphi}{\partial H} = -2\pi\,\frac{F}{H^2} .$$

In other words, the oscillation period in a magnetic field is proportional to the square of its strength and, naturally, decreases quadratically as the field decays. This suggests that oscillations become very 'fast'. Accordingly, the absolute value of χ_B may generally grow indefinitely. In this case, the increase in induction in a sample upon a change in the external magnetic field will be essentially different depending on the sign of χ_B. Indeed, this increment can be expressed as [10]

$$\delta B = \delta H + 4\pi\delta M(B) = \delta H + 4\pi\chi_B\delta B ,$$

so that the experimentally examined differential susceptibility satisfies the relation

$$4\pi\chi_H = \frac{\partial B}{\partial H} - 1 = \frac{1}{1-4\pi\chi_B} - 1 = \frac{4\pi\chi_B}{1-4\pi\chi_B} . \tag{8}$$

If $4\pi\chi_B \ll 1$, then $\chi_H \approx \chi_B$, and expression (7) holds true.

Let us consider a case of growing $|\chi_B|$. In the vicinity of $\tilde{\varepsilon}$ minimum, where $\chi_B < 0$, differential susceptibility $\chi_H \to -1/(4\pi)$ and $\partial B/\partial H \to 0$, i.e., induction B in the sample remains virtually unaltered throughout almost the entire period and $4\pi\delta M \approx -\delta H$ (much as in a superconductor). In the vicinity of $\tilde{\varepsilon}$ maximum, where $\chi_B > 0$, the denominator in expression (8) tends to vanish, χ_H increases, and the derivative $\partial B/\partial H \to \infty$ when $\chi_B \to 1/(4\pi)$, meaning that induction in the sample must increase in a stepwise fashion (Fig. 1).

Transformation of dHvA signal (Fig. 1a) into the signal shown in Fig. 1b, i.e., passage from $M(B)$ to $M(H) = M(B - 4\pi M(B))$, illustrates magnetic interaction. This trans-

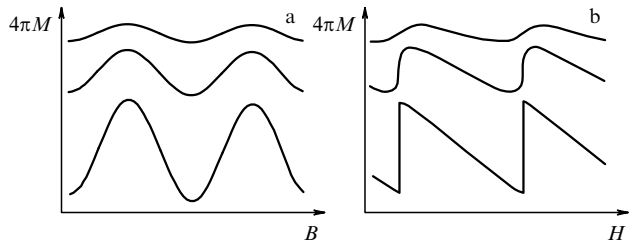

Figure 1. Transformation of the shape of magnetic moment oscillations as a result of magnetic interaction when passing from the $M(B)$ dependence, where B is magnetic field induction (a), to the experimentally examined dependence $M(H)$, where H is the external magnetic field (b). Upper, intermediate, and lower curves correspond to $a \ll 1$, $a = 1$, and $a \gg 1$, respectively [10]. Amplitude a, and hence χ_B, increase, e.g., with decreasing temperature. The dependences are shifted vertically for clearness.

formation is easy to obtain graphically in accordance with formula $B - 4\pi M(B) = H$ by simply shifting each point in the plot $4\pi M(B)$ (Fig. 1a) to the left ($M > 0$) or right ($M < 0$) by the value of its ordinate. Such a sawtooth dependence $4\pi M(H)$ with practically vertical induction steps was first observed by Shoenberg in noble metals (the Shoenberg effect) [8]. In reverse transition from $M(H)$ to $M(B) = M(H + 4\pi M(H))$, the plots are the same as in Fig. 1 for $a < 1$, but steps for $a > 1$ turn into 'gaps' corresponding to absolute instability regions (see Figs 6.1 and 6.6a in monograph [8] for comparison).

Thus, if condition

$$-\frac{\partial^2 \tilde{\varepsilon}}{\partial B^2} = \chi_B > \frac{1}{4\pi} \tag{9}$$

is fulfilled in the vicinity of maximum $\tilde{\varepsilon}(B)$ with positive susceptibility χ_B, the thermodynamic stability condition $\partial H/\partial B = 1 - 4\pi\chi_B > 0$ is not satisfied in a certain magnetic field range

$$B_1 < H < B_2\,. \tag{10}$$

This situation is illustrated in Fig. 2, where energy values in minima B_1 and B_2 become equal at $H = H_0$, and the entire absolute instability interval (10) (in a long sample parallel to the magnetic field with $n \sim 0$) is passed over at this point in a jump from state B_1 (where the minimum was for $H < H_0$) to state B_2. This is what is called the Shoenberg effect. In a plate-shaped sample normal to the field ($n \sim 1$), all B values on interval (10) corresponding to absolute instability are not realized despite the boundary condition

$$B = H \tag{11}$$

for this geometry. The state of the sample over the entire interval of the magnetic field splits into two phases corresponding to thermodynamically stable states at $B = B_1$ and $B = B_2$, with an energy gain of $\delta\varepsilon$ in the middle of this range. (Certainly, the gain is smaller if the excess energy in the domain walls is taken into account.) The requirement (11) is on the average fulfilled. The said phases are actually diamagnetic domains or Condon domains [1] with mutually opposite magnetization in neighboring phases.

It is worth noting that the phase $B_1 < H$ in Fig. 3 is diamagnetic, and the phase $B_2 > H$ is paramagnetic, although induction in both has the same direction as the external magnetic field. Magnetization current in the domain

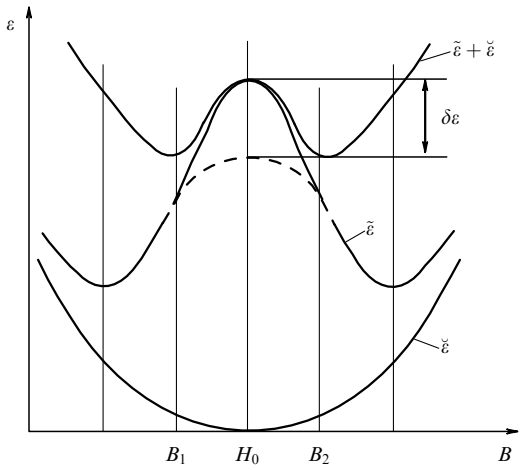

Figure 2. Energy variations as functions of induction B in a small region slightly larger than one period of oscillating function $\tilde{\varepsilon}(B)$. The external magnetic field H_0 exactly corresponds to maximum $\tilde{\varepsilon}(B)$. The lower parabola $\breve{\varepsilon} = (B - H)^2/8\pi$ represents variation of the magnetization energy for a sample with demagnetization factor $n = 0$ in the applied magnetic field H_0. The upper curve $\tilde{\varepsilon}(B) + \breve{\varepsilon}$ shows the sum (5). The case of $4\pi\chi_B > 1$ is presented with two minima appearing in expression (5) at B_1 and B_2. The energy of a plate-like sample normal to the field ($n \sim 1$) and having diamagnetic domains [10] is shown by the dashed line; $\delta\varepsilon$ is the maximum energy gain during domain formation.

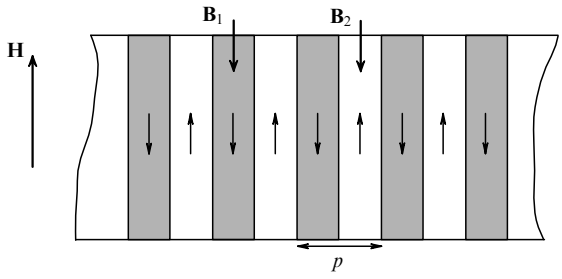

Figure 3. Schematic of the simplest laminar domain structure. Magnetic field **H** is oriented normally to the plate whose thickness d is much smaller than its size, i.e., $n \sim 1$, and the structure period p is much smaller than d.

wall ensures an induction jump $\Delta B = B_2 - B_1$. Denoting domain wall thickness by w (it is the Larmor radius in the Privorotskii theory [11–13], i.e., $w \sim R_H$), as usual we have for the period

$$p \propto \sqrt{wd}\,, \tag{12}$$

due to the competition between surface and excess energies in the domain walls [11–13]. This gives a value on the order of tens of micrometers for the usual sample thickness $d \sim 1$ mm and magnetic fields of several teslas.

Inequality (9) determines, in coordinates (H, T), the phase boundary between the region of a state with homogeneous magnetization and the region of splitting into domains formed in each dHvA period over the interval (10). For $\chi_B(B, T)$ in formula (3), the parameters of the corresponding cross section of the Fermi surface are used along with the Dingle factor $\exp[-1/(\omega\tau)]$ taking into account the broadening of Landau levels in a given sample (4).

It is easily seen that thermodynamic instability condition (9) for the case of single-harmonic approximation (when the derivative is unambiguously related to the amplitude) can be represented as the relationship between the magnetic moment

oscillation amplitude and oscillation period in the magnetic field:

$$4\pi M = \frac{P}{2\pi},$$

which represents a convenient estimate, since both quantities are directly measured in experiment.

1.3 First experiments

Condon arrived at the idea of domains [1] when analyzing magnetization measurements (the dHvA effect) in beryllium samples. Electronic pieces in the 3rd zone of the Fermi surface for this metal have an elongated cigar-like configuration. Due to this, dHvA amplitude in beryllium is high enough to ensure realization of conditions for the formation of domains in a readily accessible region of magnetic fields and temperatures. Comparing results of dHvA measurements at low temperatures in samples of different shapes might explain them on the assumption of domain appearance. Formation of domains carrying magnetization current in their walls must naturally lead to effects like supercooling and irreversible magnetization. However, all previous experiments had shown the absolute reversibility of the dHvA effect. Moreover, Condon tried to discover domain formation in a single-crystalline beryllium plate by measuring magnetic field distribution in the immediate proximity to the sample surface by a point sensor. However, this method failed to confirm the formation of domains in beryllium.

The confirmation was for the first time obtained two years later by measuring NMR in silver [14]. Results of this experiment are presented in Fig. 4. The high-frequency (≈ 20 MHz) signal was absorbed in a thin surface layer, at the depth of the skin layer (about 1 μm). In the case of homogeneous magnetization of the crystal, a single line corresponding to the strength of the applied magnetic field was apparent. Domain formation was accompanied by periodic splitting of the line (see Fig. 4).

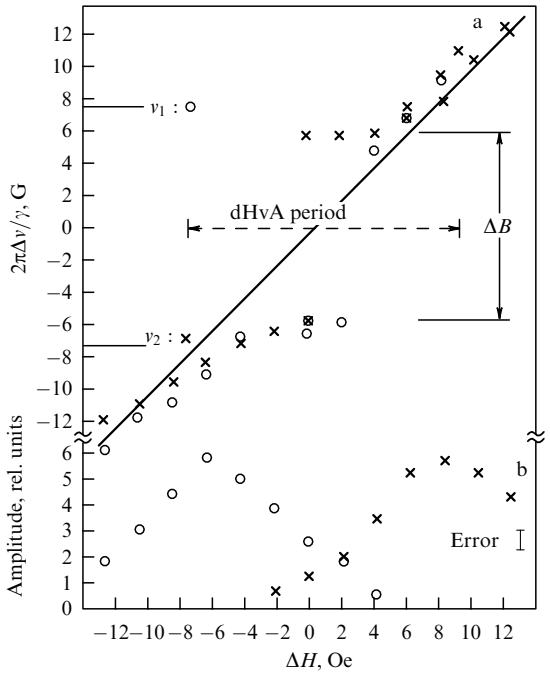

Figure 4. Frequencies (a) and amplitudes (b) of NMR peaks on a silver single-crystalline plate in the 9 T magnetic field at 1.4 K in a range of around one dHvA period. Line splitting at the center of the period, corresponding to a domain emergence, amounted to approximately 12 G, i.e., about a dHvA half-period. (b) Variation of the peak intensities corresponds to variation of the phase volumes.

Paradoxically, similar experiments on beryllium that were expected to reveal an even greater effect led to no result. The explanation offered by the authors and based largely on beryllium NMR quadrupole splitting (magnetic moments of beryllium and silver nuclei being 3/2 and 1/2, respectively) was for a long time the only one. We believe that the true cause is much deeper than that (see Section 3.2).

Nevertheless, diamagnetic domains in beryllium also manifested themselves as magnetic field dependences of resistance or thermopower oscillation amplitudes, characteristic of this metal. To recall, magnetic breakdown in beryllium substantially increases these amplitudes. A specific feature of the Fermi surface in beryllium is that the thickness of the layer of open trajectories resulting from the magnetic breakdown in the basal plane between the cigar-shaped electronic structure in the 3rd zone and the hole 'coronet' in the 2nd one equates with the thickness of the thin coronet necks. This narrow layer of open trajectories is consistent with the cigar cross section determining the period of oscillations and practically coinciding with the central cross section. It is for this reason that beryllium is characterized by a huge amplitude of magnetic breakdown oscillations of resistance and thermopower, whose magnetic frequency is determined by the central cross section of the cigar [15].

However, the cigar also possesses two symmetric noncentral (extremal) cross sections, besides the central one, from which they differ by 3% in terms of the area. These two cross sections are apart one quarter of the cigar length from the basal plane [16], and therefore do not participate in the formation of magnetic breakdown trajectories and respective giant oscillations. As a result, the dHvA frequency is a function of the noncentral cross section, and beats take place. The oscillation amplitude undergoes periodic 3-fold variations, with the frequency of magnetic breakdown oscillations being smaller by the same 3%. As a consequence of peculiar interference, sites of instability $\Delta B = B_2 - B_1$ periodically formed in a sample with the dHvA frequency, in which all intermediate induction values fail to be realized, coincide in turn with the minima and maxima of magnetic breakdown oscillations of resistance or thermopower; the alternation occurs with the same beat period. Such a beat-periodic alternative 'excision' of oscillation minima and maxima replaces the monotonic increase in the magnetic breakdown oscillation amplitude with growing magnetic field due to the enhanced probability of magnetic breakdown [17]. The appearance of such an envelope of the amplitude of magnetic breakdown oscillations of resistance or thermopower in beryllium with lowering temperature had to give evidence of the formation of diamagnetic domains.

No other experiment demonstrating formation of Condon domains was reported for many years (1968–1996). An exception that more likely proves the rule is the work of Bozhko and Vol'skii [18, 19]. The authors interpreted the anomalous helicon behavior they observed in aluminium at low temperature ($T < 1$ K) as a result of the formation of diamagnetic domains. Furthermore, some hard-to-explain results of silver experiments were also attributed to the formation of Condon domains [20, 21]. Not surprisingly, diamagnetic domains were regarded as a very rare if not exotic phenomenon, although they remained in the focus of

interest of researchers. Many theoretical studies concerning different aspects of this phenomenon were carried out during a rather long period [22–28].

One more aspect of the problem of diamagnetic instability formation is worthy of note here. Touching the Fermi surface by the next successive Landau level upon reduction of the magnetic field and subsequent occupation of this level by electrons can be formally regarded as the formation of a new void, i.e., the $2^1/_2$-order phase transition (Lifshits transition) with inherent singularity in the density of states [29] and corresponding peculiarities in thermodynamics and kinetic coefficients. As known, this phase transition is 'smeared' [30] due both to finite temperature and scattering by impurities (the finite Dingle temperature). However, when approaching an 'ideal' situation (i.e., at both T and T_D approaching zero), singularity can be cancelled by virtue of developing instability at the contact point and formation of diamagnetic domains in its vicinity [31]. Generally speaking, this fact alone is enough to suppose that Condon domains can form practically in any metal under suitable conditions.

2. Muons in diamagnetic domain research

Progress in experimental studies of Condon domains has been achieved by applying positive muons to the local measurement of magnetic induction in a sample. Muons are unstable elementary particles with the lifetime $\tau_\mu = 2.19714 \times 10^{-6}$ s and spin 1/2. A beam of positive muons is generated in an accelerator by bombarding a target with high-energy protons that interact with the nuclei giving first rise to $\pi^\pm$-mesons (pions). Thereafter, positive and negative muons are produced in a nuclear reaction of pion decay into a muon and neutrino: $\pi^+ \to \mu^+ + \nu_\mu$. In a sample, the muon spin precesses in the surrounding local magnetic field, and the muon lifetime is long enough to allow for the reasonably exact measurement of the precession frequency and, therefore, the field intensity. Given a sample with two phases with different inductions, two values of precession frequency will be obtained in this way.

2.1 General characteristic and description of the method

The muon spin rotation (μSR) method [32] developed at the interface of two sciences, nuclear physics and condensed matter physics, is in a sense analogous to the NMR technique. In both cases, induction is measured from spin precession frequency in a magnetic field. However, important differences should be specified. First, the nuclear spin in certain metals is other than 1/2, which makes difficult NMR measurement. For example, quadrupole splitting occurs in beryllium, while most tin isotopes have no nuclear moment whatever. There is no such problem with the μSR method because one and the same 'nucleus', a muon with the mass $m_\mu = 206.77 m_e$ (m_e is the electron mass) and hyromagnetic ratio $\gamma_\mu = 2\pi \times 13.554$ kHz G^{-1}, is used for all metals. Since the precession frequency is being measured directly (see below), a high-frequency electromagnetic field that penetrates into the metal only as deep as the skin layer is unnecessary. Therefore, resonant absorption (hence, the measurement of induction) in the NMR method is confined to the thin surface layer. In contrast, muons penetrate rather deep into the sample. Because of this, the μSR method makes it possible to characterize the bulk properties of the sample. This second important advantage of μSR method over NMR technique was later shown to be crucial in the context of beryllium research.

As early as 1979, Yu M Belousov and V P Smilga proposed applying the μSR method for observation of Condon domains [33, 34]. Unfortunately, their work long remained unnoticed. Only after 16 years was the method used for this purpose at the Paul Scherrer Institute, Switzerland. Beryllium experiments were successfully completed in 1995 when the formation of Condon domains was observed in the form of μSR-peak splitting, as in the NMR method [35].

The μSR method for direct measurement of precession frequency and, consequently, the local field is essentially as follows. A muon beam passes through a collimator and hits a sample placed in a homogeneous magnetic field. The beam diameter is around 6 mm or, as a rule, slightly smaller than the sample size. A special inlet device rotates the muon's spin by approximately 90°, so that spins of all muons in the sample are initially oriented in a similar way, vertically and perpendicular to the horizontal magnetic field. Muon thermalization time, i.e., the time before the particle 'stops', is negligibly small, which makes all muons begin to precess simultaneously. Muon penetration depth depends on the momentum value (in the present case ≈ 28 MeV/c) and sample matter density. It is different for various metals but always smaller than the sample thickness. After the muon is 'stopped', it diffuses within a certain region, the size of which is at least a few orders of magnitude smaller than the possible domain length. At this time, muon spin precesses in accordance with the local field strength up to the instant of decay:

$$\mu^+ \to e^+ + \nu_e + \tilde{\nu}_\mu \,,$$

where e^+ is the positron, ν_e is the electron neutrino, and $\tilde{\nu}_\mu$ is the muon antineutrino.

Due to decay asymmetry, a positron usually escapes in the muon spin direction and is recorded by the appropriate positron detector. This permits determining the precession time and final direction of the muon spin. The experiment is designed so as to measure the event during which the sample contains exactly one muon throughout the entire precession time. The event is discarded if another muon enters the sample before the preceding one decays. In a different modification of the experiment using the MORE (muon-on-request) technique, the beam is shut off as soon as the scintillator fixes that the sample is 'occupied'. This approach is more preferred because it permits a faster collection of the necessary number of events (statistics) and produces less noise. Moreover, 'extra' muons can be simultaneously utilized in the adjacent spectrometer.

Thus, registering of huge numbers of positrons ($\sim 10^6$ or more) exposes the oscillatory dependence $N(t)$ corresponding to muon spin precession in a given field, provided it is sufficiently homogeneous throughout the sample's active area. If two phases with different magnetic inductions are formed, these frequencies are resolved by Fourier analysis providing the difference, ΔB, is large enough. In other words, a homogeneously magnetized sample must exhibit, as in the NMR method, a single very narrow peak that must split in the presence of domains. Two positron detectors (left and right) were usually employed with a phase shift of π between them. Histograms of the two detectors are slightly different due to the dissimilarity of their technical characteristics, allowing for their analysis separately or as a whole. Thus, we have

$$N_i(t) = N_{0i} \exp\left(-\frac{t}{\tau_\mu}\right)\left[1 + AP_i(t)\right] + b_i \,,$$

where $i = 1, 2$ is the detector number, the decay exponent with the muon lifetime $\tau_\mu = 2.19714$ μs determines the time interval for the measurement, and b_i is the noise level. The constant of muon decay anisotropy, assuming positron escape along the spin direction as the essence of the method and averaging over the positron energy, may be defined as $A = 1/3$. In this experimental design, time-dependent muon polarization $P(t)$ perpendicular to **B** oscillates with the frequency $\omega = \gamma_\mu B$ and decreasing amplitude because muon precession occurs in a nonideally homogeneous field. There are always several causes leading to inhomogeneity of the magnetic field in which muon precession proceeds. In a real lattice, even in case of an ideally homogeneous magnetic field, diffusion enables the muon to 'visit' different interstitial lattice sites and 'watch' nuclear magnetic moments randomly oriented at a given temperature and an external magnetic field. As a result, we have for homogeneous magnetization

$$P_i(t, H) = \exp(-\lambda t)\cos(\gamma_\mu B t + \phi_i), \quad i = 1, 2, \tag{13}$$

where the phases in detectors 1 and 2 equal 0 and π, respectively. Here, $B = B(H)$ takes account of sample magnetization. The damping constant λ is a result of the superposition of all factors responsible for field inhomogeneity. The contribution to λ related to the aforementioned random direction of nuclear spins (determined by muon diffusion over interstitial sites) is significantly different in various metals. Moreover, inhomogeneous magnetization of the sample, for example, due to deviation of the sample shape from the ellipsoidal one, can also lead to a slight enhancement of damping.

As a rule, the value of λ in our experiments, related to the character of muon diffusion alone (without regard for magnetization), varied from 3 to 30×10^4 s^{-1}, which made possible revealing the formation of phases with different precession frequencies, i.e., diamagnetic domains, in all the experiments. Inhomogeneity of the external magnetic field was then absolutely unessential. First, the inhomogeneity, small in itself, was in addition one order of magnitude smaller than the dHvA period within the sample active area. Second, the transition into the two-phase state is a transition to a state with two domains having inductions B_1 and B_2. Therefore, the presence of even a small field gradient may influence only the shift of interface between the phases. In other words, values B_1 and B_2 in the domains become stabilized as usual in phase transitions. Certainly, we are not speaking about the domain structure, i.e., domain shape and size. These issues are beyond the scope of a muon experiment.

To sum up, in the ideal case (in the sense that the domain wall volume is negligibly small), polarization in the positron detector assumes the form

$$P(t) = \sum_{j=1,2} a^j(H)\exp(-\lambda t)\cos(\gamma_\mu B_j t + \phi_j). \tag{14}$$

Here, phases ϕ_j equal 0 and π for the first and second detectors, respectively. Unlike the field-dependent frequency in formula (13), frequencies $\gamma_\mu B_1$ and $\gamma_\mu B_2$ in formula (14) correspond to dia- and paramagnetic phases and do not change over the entire domain existence region. The positions of muons that happen to enter domains being randomly distributed, the amplitudes $a^1(H)$ and $a^2(H)$ exactly correspond to the volumes of dia- and paramagnetic phases.

The real situation is quite different from the ideal one. As mentioned above, even in the case of homogeneous magnetization, the damping constant λ is equivalent to the broadening of the μSR peak in frequency $\Delta\nu \approx \lambda/\pi$ or, correspondingly, to the broadening of $\Delta H = 2\pi\Delta\nu/\gamma_\mu$ in the field. Moreover, the interdomain boundaries in the two-phase state occupy a part of the sample volume that is far from being negligibly small. As it has turned out at a later time (see Section 3.2), the thickness of the domain wall is an order of magnitude greater than the Larmor diameter of the electron orbit, whereas early authors assumed these parameters to be of the same order [11–13]. This means that a large fraction of muons in a sample will precess with frequencies more or less equally distributed over the interval between $\gamma_\mu B_1$ and $\gamma_\mu B_2$.

Thus, there is every reason to expect that markedly broadened peaks in a real sample will overlap so that their resolution by the method under consideration is virtually impossible. In other words, the time window is not large enough to observe frequency beats, when induction values in domain phases B_1 and B_2 are rather similar and, consequently, the beat period is much greater than the muon lifetime. This, however, does not preclude observation of Condon domain formation within a given range of magnetic fields. The emergence of two close peaks instead of a single one is manifested as peak broadening and, accordingly, increased λ. This becomes apparent when experimental histograms are fitted with formula (13), assuming $\lambda = \lambda(H)$ and remaining $B = B(H)$. The appearance of the second (new) magnetization phase stands in this case for the enhanced inhomogeneity of B. Then, domain formation results in function $\lambda = \lambda(H)$ oscillating in the magnetic field, and its oscillation period must exactly coincide with the dHvA period well-known in advance for a given crystal with a given orientation. Clearly, such oscillations can be induced by no other causes, including oscillations of ordinary inhomogeneity in B distribution due to magnetization currents and deviation of the sample shape from the ellipsoidal one (see above); otherwise, λ would undergo double-frequency oscillations.

To sum up, oscillations of damping constant $\lambda = \lambda(H)$ with a 'right' period unambiguously points to the presence of diamagnetic domains in the sample, while the position of the λ maximum coincides with the middle of the domain region and the maximum λ value may be used to roughly estimate the splitting $\Delta B = 2\lambda/\gamma_\mu$ from formula $\Delta\nu \approx \lambda/\pi$ (see above). Looking ahead, it can be noted that it is in this way that Condon domains were detected in all studied crystals of beryllium, tin, lead, indium, and aluminium [36, 37]. Only in two of these metals, beryllium and tin, was it possible to measure splitting directly by the spectroscopic method; in other words, peak splitting was revealed by fitting with formula (14) as a result of beating.

It should be emphasized that in the 'ideal' situation with low noise b and damping constant λ and high splitting $\Delta\nu$, domains in the Fourier spectrum correspond to two well-separated narrow peaks. In such a situation, it would be possible, in principle, to estimate the sample volume occupied by the interdomain walls (from filling the interpeak gap in the spectrum) and thereby to roughly determine wall thickness. This problem can be addressed in a somewhat different way. Setting the induction distribution profile in the wall as an adjustable parameter and comparing the result obtained with experimental findings permit us to reach the best coincidence. Such calculations were made for beryllium in Ref. [38]. Unfortunately, the situation proved far from ideal. The result

(much higher than 10% of the period) may be considered only qualitative.

To conclude, the μSR method allows the presence of Condon domains to be unambiguously established, but its application to the elucidation of the detailed domain structure is a subject of future research.

2.2 Measurements in beryllium

Muon precession was measured with an LTF (Low Temperature Facility) μSR spectrometer at the Paul Scherrer Institute, Switzerland. The superconducting solenoid generated a roughly 2.9-T horizontal magnetic field. A muon beam directed along the solenoid axis entered the sample through the collimator and a vacuum window. The sample was placed in a vacuum and attached to a silver holder that was in thermal contact with a dilution cryostat. This experimental setup permitted creating and maintaining constant temperature over a wide range from 4.2 K to approximately 20–30 mK. Measurements were made under two regimes: at 'high' (4.2–1.5 K) or low (0.8 to 20–30 mK) temperatures. Passage from one regime to the other took a specific time. Both were used in beryllium experiments alone, while experiments with other metals were carried out only at low temperatures.

The samples were single-crystalline plates oriented one way or another relative to the magnetic field direction; their size (10–12 mm) was significantly greater than the muon beam divergence. Due to this, the majority of muons entered the sample and underwent precession. The outgoing positrons (products of muon decay) were registered by two detectors placed on the left and on the right of the beam. A small fraction of the muons could stop outside the sample and created a certain background in all timing channels and therefore impaired the resolution power. Nevertheless, definitive results were obtained in all experiments. Sample thickness was chosen so as to ensure that muons penetrated the metal to a depth smaller than this thickness.

The lower part of the holder had a four-contact socket to connect it to the sample. It made possible *in situ* measurements of either resistance or thermopower of the sample. Such measurements were necessary in the early beryllium experiments for independent control of the presence of domains. They were not made in later studies.

The first muon experiments were carry out on beryllium [35]. The dHvA amplitude in beryllium is maximum in the direction of the magnetic field parallel to the hexagonal axis. Such a situation (see Section 1.3) is attributable to the cigar-shaped electronic piece of the Fermi surface in the 3d zone. The cigar has three extremal cross sections: a central one with $F = 9.44 \times 10^2$ T, and two symmetric noncentral ones with $F = 9.71 \times 10^2$ T [39, 40]. All of them possess a similar curvature. Hence, the characteristic amplitude beats present in dHvA oscillations with a period encompassing roughly 33 high-frequency periods; the amplitude from nodes to antinodes varies threefold. Due to developing instability, diamagnetic domains form in antinodes at a higher temperature. The position of antinodes in a magnetic field is well known, which essentially facilitated correctly choosing the magnetic field range in a prolonged and expensive muon experiment.

In addition, thermopower oscillations were measured *in situ* in the first experiment since it was *a priori* known that in a sample of a given shape such measurements dissipate power almost one order of magnitude smaller than that dissipated by measurements of resistance at the same magnitude of the signal measured.

As mentioned in Section 1.3, the analysis of magnetic breakdown oscillations reveals domain state formation in a crystal. To recall, the described procedure of continuous sample quality control intended for the observation of diamagnetic domain formation using muon spin rotation method was deemed necessary in the first LTF-based experiments because of the extremely high cost of the beam time; it could not be used for duplicate measurements and the result was difficult to predict.

The beryllium sample constituted a plate measuring $9 \times 10 \times 1.8$ mm. Its demagnetization factor ($n \approx 0.77$) was assumed to be identical with that of an ellipsoid with 9-, 10-, and 18-mm axes inscribed into the sample [41]. The normal to the plate coincided with the hexagonal axis of the crystal. The plate was cut out from a bigger crystal by electrospark erosion. Resistance ratio was $R_{300\,\mathrm{K}}/R_{4.2\,\mathrm{K}} \approx 300$, and the Dingle temperature $T_\mathrm{D} = 2.2$ K. The magnetic field range was slightly broader than two dHvA periods in the oscillation antinode region. The period in this magnetic field was roughly 44 G (Fig. 5). Field instability in a time (around 1 hour) of measurement of one histogram, i.e., a single point in the plot, did not exceed 1 G; the same is true of magnetic field inhomogeneity within the sample. Taken together, these parameters ensured sufficiently accurate measurement.

The data presented in Fig. 5 are adequately described by formula (13) only for homogeneous magnetization segments, i.e., in the vicinity of the λ minimum. Doubtless, the observed periodic enhancement of λ reflects a broadening of the μSR peak, although, strictly speaking, formula (13) in such a situation is in conflict with reality. This broadening happening exactly in conformity with the 'correct' dHvA period indisputably suggests the emergence of diamagnetic domains. In other words, domain formation produces two peaks, either well resolved (a doublet) or overlapped so (for a variety of reasons) that the doublet escapes resolution and only oscillations of λ can be observed. In the μSR spectra thus obtained and measured in dHvA oscillation antinodes for temperatures $T < 0.5$ K, a well-apparent split doublet can be seen in magnetic fields up to $H = 1.5$ T. However, in beat nodes, where the amplitude of dHvA oscillations is three

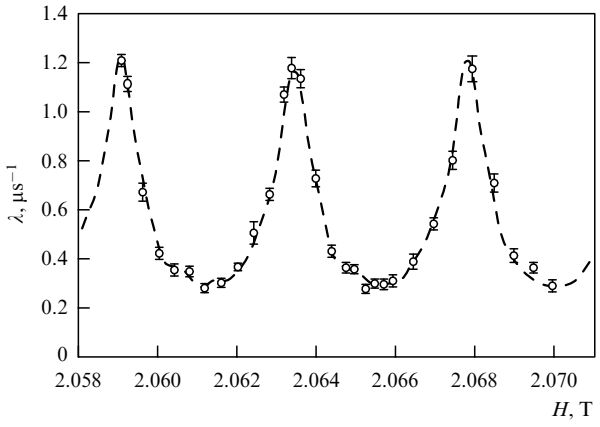

Figure 5. Dependence of the damping constant λ on the applied magnetic field H deduced from experimental histograms using formula (13) at temperature $T = 0.5$ K. Sharp rise in λ with a period of 44 G is unambiguously interpreted as periodic domain formation with the peak splitting $\gamma_\mu \Delta B = 2\lambda \approx 0.5$ MHz.

times smaller, only a periodic increase in λ is observed, which also suggests domain formation.

After the magnetic field decreases to below 1 T, nothing in μSR spectra points to the presence of domains. However, this gives no reason to think that the phase boundary for domain existence that we have crossed passes here. Indeed, the oscillation period amounts to $\Delta H = H^2/F \sim 10$ G at $H = 1$ T and possible splitting is roughly 5 G, i.e., the beat period is about 15 μs, corresponding to the maximum value of $\lambda \sim 0.2\ \mu s^{-1}$. Such a value is difficult to record, not only because the muon life-time is too short for that, but also because λ has approximately the same value, even in the homogeneous phase of the sample.

Thus, large λ both in Fig. 5 and in subsequent reports [35, 42, 43] unambiguously suggests the formation of two phases with different induction values, B_1 and B_2, and, accordingly, different precession frequencies as follows from the results of histogram fitting with formula (14). The Fourier transform of the depolarization function (14) in the vicinity of the λ maximum in Fig. 5 at $H = 20{,}634$ G revealed the presence of the doublet in all spectra with $B_1 = 20{,}607$ G and $B_2 = 20{,}643$ G.

Figure 6 depicts Fourier spectra for 5 histograms in magnetic fields (from top to bottom) $H = 20{,}640$, 20,636, 20,634, 20,632, and 20,628 G. (For the purpose of display, the spectra are shown in two figures (a and b), with the central spectrum for $H = 20{,}634$ G presenting in both.) The right, paramagnetic, peak decreases with decreasing magnetic field, while the left, diamagnetic, one increases, in conformity with the changes in phase volumes. Peak amplitudes in the center of the domain two-phase region are virtually identical.

Figure 7 presents results of $B(H)$ measurement within a wider range of magnetic fields, encompassing more than two dHvA periods in the same oscillation antinode region as in Figs 5, 6. In regions with homogeneous magnetization, $B(H)$ is a single-valued function corresponding to one peak. Formation of diamagnetic domains is accompanied by the appearance of a doublet and, accordingly, B_1 and B_2 values.

For comparison, measurements were made at a small shift of the magnetic field strength into the region of the nearest dHvA oscillation beat node (toward the antinode in Fig. 7). The results of these measurements given in Fig. 8 emphasize a very convenient property of beryllium: the ability to significantly change (due to beating) the oscillation amplitude in a practically 'invariable' magnetic field. As follows from Fig. 8,

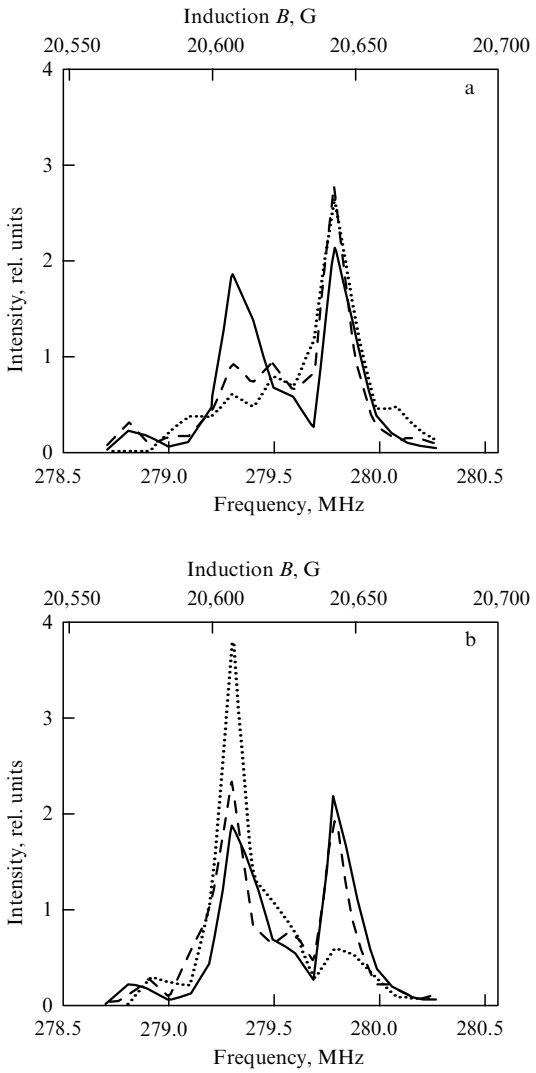

Figure 6. Splitting of μSR spectra in a dHvA antinode in the vicinity of $H = 20{,}634$ G at $T = 0.5$ K: (a) $H = 20{,}640$ G (dotted line), $H = 20{,}636$ G (dashed line), and $H = 20{,}634$ G (solid line); (b) $H = 20{,}634$ G (solid line), $H = 20{,}632$ G (dashed line), and $H = 20{,}628$ (dotted line). Position of peaks of respective dia- and paramagnetic phases, $B_1 = 20{,}607$ G and $B_2 = 20643$ G, remains unaltered. The volume of para- and diamagnetic phases decreases and increases, respectively, with a reduction in the magnetic field.

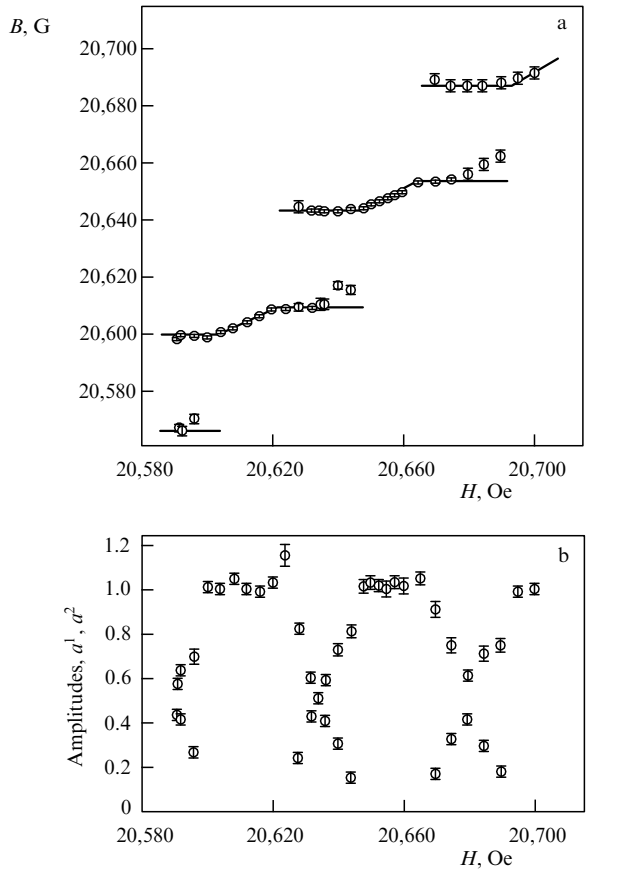

Figure 7. (a) Induction B in a beryllium sample measured by the spectroscopic method at $T = 0.5$ K. Solid line — calculation for $n = 0.775$ [42]. (b) Peak intensities a^1, a^2 from formula (14). In the doublet region, a^1, a^2 vary linearly with the magnetic field, strictly in conformity with changing phase volumes.

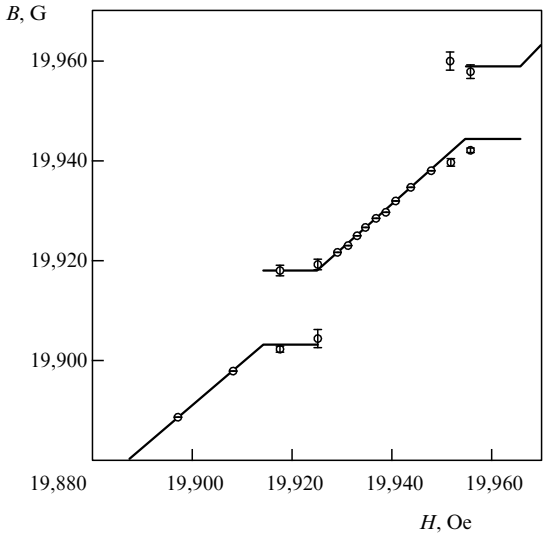

Figure 8. Induction $B(H)$ in the oscillation node adjacent to the one shown in Fig. 7, where the dHvA amplitude is three times smaller. Temperature $T = 0.5$K. Solid line depicts the result of calculations at $n = 0.775$ [42].

the period remained virtually unaltered, but peak splitting and the domain region decreased almost twofold, whereas the homogeneous magnetization region increased accordingly.

All results shown in Figs 5–8 were obtained in decreasing magnetic fields. It was interesting to compare them with the results of analogous measurements in increasing magnetic fields. In principle, it gave an opportunity to find hysteresis that could be expected for the same reasons as supercooling characteristic of first-order phase transitions during measurements at varying temperatures. The reciprocal field change was confined to a narrow range (within one dHvA period) in order to reduce to a minimum the magnetic field strength shift due to intrinsic hysteresis of the superconducting solenoid.

These experiments showed that the irreversibility of dHvA magnetization is at least no more than 2 G, i.e., below the resolving power of the method. Looking ahead, it can be noted that more accurate measurements of hysteresis by other methods (see Section 5) yielded a similar value.

Accurate determination of phase diagrams implies the exact detection of transition from the homogeneous to the domain state. It requires a reliable measurement of splitting ΔB as $\Delta B \to 0$, i.e., in the region where the μSR method does not work. Nevertheless, results obtained when crossing the phase boundary upon a change in both H and T may be worth taking into account, even if with some reservation.

Finding the phase boundary from the temperature variation is illustrated in Fig. 9. A change in $\Delta B(T)$ was measured in a constant magnetic field ($H = 2.642$ T) corresponding to the middle of the domain region, i.e., $\lambda_{\max}$ in an oscillation antinode. Measurements were made during both decreasing and increasing temperatures (see Fig. 9). Unfortunately, their accuracy in this experimental layout (unlike that of measurements in a varying magnetic field) precludes any definitive conclusion as regards the degree of supercooling. The best agreement with the theory is obtained for the phase boundary at point $T_0 = 3.0$ K. The last points at $T = 3.5$ K should be discarded as unconvincing, as was also noticed when fitting histograms with formula (13).

To sum up, Condon domains in beryllium were discovered and studied by the μSR method in a range of magnetic

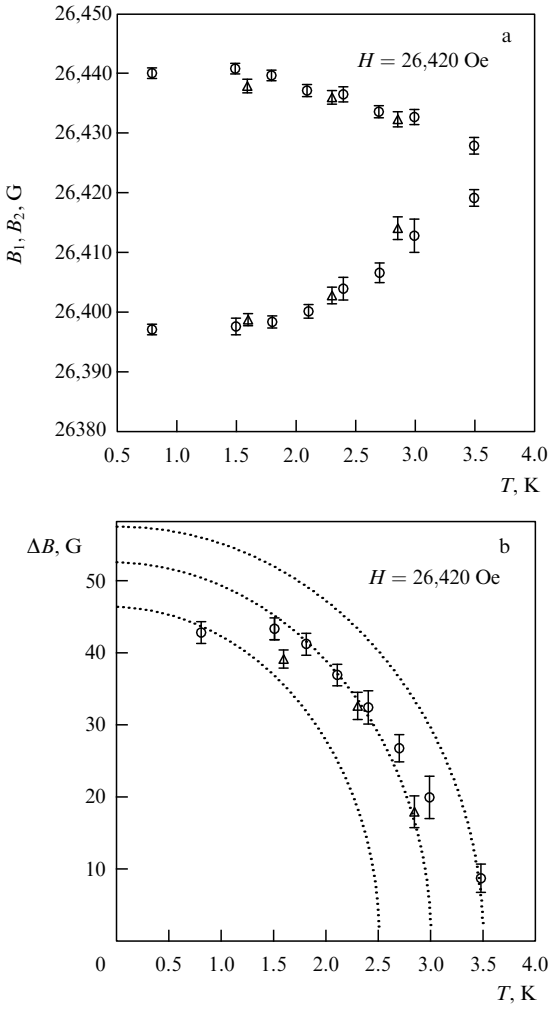

Figure 9. (a) Measurement of the doublet B_1, B_2 at $H = 2.642$ T corresponding to the middle of the dHvA period, viz, $\lambda_{\max}$, during heating (circles) and cooling (triangles). The resolution of two frequencies, i.e., two values of magnetic induction at $T = 3.5$ K, seems to be difficult. (b) Temperature dependence of ΔB. Dotted curves display calculated dependences in the first-harmonic approximation with the phase boundary T_0 as a parameter chosen to equal 2.5, 3.0, and 3.5 K, respectively.

fields up to 3 T and temperatures up to 0.1 K. Concurrently, the ΔB splittings and phase boundary positions were found. The dHvA amplitude was shown to be much greater than predicted by the LK formula. Taken together, these findings confirm the result we obtained earlier [40] by measuring the dHvA effect in beryllium with a Hall probe.

2.3 Diamagnetic domains in metals with a small de Haas–van Alphen amplitude

Diamagnetic domains in both silver and beryllium were observed under conditions when the dHvA amplitude was close to or even greater than the oscillation period. In this case, instability and, as a result, Condon domains explicitly develop in the single-harmonic approximation (see Section 1.2). Such an approach is fully justified when temperatures are not too low. However, the dHvA amplitude in most metals is significantly smaller and, moreover, always remains significantly smaller than the oscillation period, even in samples of highest quality [44] and at extremely low temperatures. Therefore, it might be supposed that magnetic interaction is unessential in this case, and Condon domains

cannot form. In the framework of this approach, the emergence of Condon domains would be, in fact, a very rare, exotic phenomenon. But the stability condition (9) is, strictly speaking, determined by the second derivative that, in the general case, can be large despite the small magnetic moment amplitude. In principle, this conclusion ensues from the analysis of the LK formula taking into account higher harmonics. However, such a procedure is too cumbersome.

The following line of reasoning (see Section 1.3) appears equally convincing but much more demonstrative. Indeed, touching the Fermi surface by the next successive Landau level may be interpreted as giving rise to a new band, i.e., as an electronic topological transition with the formation of singularity in the density of states at $T = 0$ (I M Lifshits [29]). Then, it is easy to see that the second derivative is determined first and foremost by the number of the Landau level rather than by the extremal belt width, i.e., Fermi surface curvature at the contact point and, accordingly, dHvA amplitude. Therefore, inequality (9) when T, $T_D \to 0$ can be fulfilled if this number exceeds a certain critical value (equal to $\sim 10^3$ in the free-electron model). In other words, instability and splitting into Condon domains always occur as T, $T_D \to 0$ for any Fermi surface and any extremal belt.

In light of the foregoing, it was interesting to search for diamagnetic domains in metals having Fermi surface cross sections consistent with this magnetic field region by the μSR method using an LTF spectrometer (limiting temperature ≈ 20 mK, and magnetic field up to 3 T). Naturally, it required single crystals of the highest quality and their proper orientation. Tin, aluminium, lead, and indium single crystals were grown at the P L Kapitza Institute for Physical Problems, RAS 40 years ago. [1]

2.3.1 Tin. Tin has a very complicated Fermi surface composed of several sheets in the 4th, 5th, and 6th Brillouin zones [45–53]. In other words, there is a wide choice of cross sections (including small ones) and thus dHvA periods for obtaining a large enough period in low magnetic fields ($H < 3$ T). Moreover, the natural tin of which the single crystal consists contains very few isotopes (ca. 12%) with a nuclear magnetic moment. For this reason, self-attenuation λ in tin due to the random magnetic field created by the adjacent nuclei is extremely low. So, it is almost 10 times lower than in beryllium, and much lower than in other metals. This gives an opportunity, in principle, to 'see' the formation of domains with extremely small splitting ΔB.

Measurements were carried out using an $18 \times 12 \times 0.56$-mm tin single crystal prepared from a disk 18 mm in diameter by etching 'redundant' segments in a diluted acid. The residual electron free path in the starting single crystal was a few millimeters [54], which testifies to its high quality. The Dingle temperature in the sample did not exceed 0.1 K, and the normal to the plate coincided with axis (100). Of the large set of low-frequency cross sections for such magnetic field orientation, two appear especially attractive. These are the 'molar tooth' cross section in the 6th Brillouin zone at the Fermi surface with the effective mass $m^*/m = 0.29$ [51] and frequency $F_1 = 446.8$ T [53], and the cross section in the 5th zone with m^*/m around 0.6–0.7 and frequency $F_2 = 2080$ T [45, 51–53].

[1] I thank V F Gantmakher and V S Edel'man for the gift of high-quality single crystals.

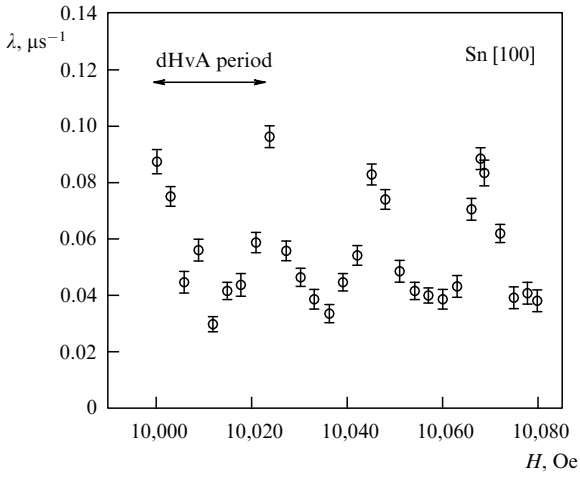

Figure 10. Periodic changes in damping constant $\lambda(H)$ at $T = 0.08$ K. The observed period $\Delta H = 23$ G exactly coincides with that for F_1 in the given magnetic field. The observed amplitude of λ corresponds to the formation of a domain structure with $\Delta B = 2\lambda/\gamma_\mu = 2.5$ G (an order of magnitude smaller than the period).

Figure 10 demonstrates $\lambda(H)$ oscillations associated with domain formation in the tin sample under consideration. Worthy of note is the extremely low damping level in the homogeneous region: $\lambda_u = 0.03$ μs^{-1}. It is a result of the aforementioned properties of tin and of applying the new MORE technique (see Section 2.1) that was regrettably unavailable at the time of experimenting with beryllium.

It is this that allowed such a small value of $\Delta B = 2.5$ G to be determined. The picture remained qualitatively unaltered with an increasing magnetic field up to 1.41 T; only the period increased twofold (to $\Delta H = 46$ G, in accordance with the formula $\Delta H = H^2/F$). Simultaneously, λ rose to 0.14 μs^{-1}, which is still insufficient for explicit doublet resolution. Regular alternation of sharp rises and falls in λ over more than 100 periods cannot be interpreted as anything but Condon domain formation. As expected, splitting ΔB was always some 10 times smaller than the dHvA period. It is absolutely out of the question in the single-harmonic approximation in which ΔB rapidly becomes as large as a half-period or greater upon crossing the phase boundary. The observed picture exactly corresponds to the situation in which the dHvA amplitude is much smaller than the half-period. Clearly, the Shoenberg effect (sawtooth dependence $4\pi M(H)$ with the same jumps $\Delta B = 2.5$ G) would be observed in a sample with the demagnetization factor $n \sim 0$ under the same conditions, i.e., at the same temperature, magnetic field strength, and Dingle temperature. This inference is in line with dHvA effect magnitudes measured on the same cross section in a tin sample of similar quality in the same magnetic field region [44, 48].

As mentioned in Section 1.1, the dHvA amplitude in the single-harmonic approximation at a critical point $4\pi\chi_B = 1$ is defined by the following expression

$$4\pi M = \frac{P}{2\pi},$$

where P is the oscillation period in a given magnetic field. In other words, the dHvA amplitude must reach at least ≈ 3.5 G for domain formation to occur at $P \approx 22$ G. However, the experimentally found amplitude in the case is 10 times

smaller. Therefore, the data obtained give definitive evidence that instability develops and domains form due to the contribution of higher harmonics alone.

As the magnetic field grows, higher frequencies begin to play an increasingly greater role in the region of $H = 2$ T, and mixing of two oscillation periods, usual for the dHvA effect, can be observed. Starting from $H \approx 2.6$ T, the second frequency $F_2 = 2080$ T becomes predominant with the period $\Delta H = 33.3$ G in this field (Fig. 11).

Maximum damping constant $\lambda = 0.4\ \mu s^{-1}$ in Fig. 11 corresponds to the value of $\Delta B \approx 9$ G, which is already high enough for doublet resolution. Figure 12 presents results of histogram fitting with formula (14).

Splitting (≈ 8 G) in Fig. 12 is still much smaller than necessary in the single-harmonic approximation. Therefore, domain formation in this case, too, requires a substantial contribution of higher harmonics to the dependence $\tilde{\varepsilon}(B)$ and, accordingly, to the dependence $M(B)$ that becomes saw-toothed with moment jumps much smaller than the half-period. (To recall, in the single-harmonic approximation, the magnetic moment becomes a sawtooth function in the passage from $M(B)$ to $(M(H)$ only if the dHvA amplitude from one peak to another satisfies the condition $8\pi M_{\max} \geqslant P/\pi \approx 11$ G.)

Worthy of note is the qualitative specificity of domain formation in tin. Unlike B_1 and B_2 values in beryllium and silver, which are essentially constant over the entire region of separating into domains, they shift in tin along the entire domain region almost in proportion to magnetic field shift. Unfortunately, this is a very weak effect, on the verge of the resolving power of the method. Therefore, no simple explanation for it has been offered thus far. Nevertheless, phase volumes change linearly with the magnetic field, as in the classical case (Fig. 13).

ΔB decreases with rising temperature, and domains disappear after crossing the phase boundary. Damping constant $\lambda_{\max}$ was measured for both cross sections in the region of $T < 1$ K (Fig. 14).

Results shown in Fig. 14 are in line with the above inference (domains disappear at a much lower temperature than in silver and beryllium). It is possible to roughly specify the positions of two points at the phase boundary in the phase diagram drawn on the (H, T) coordinates: (1 T, ≈ 0.5 K) and (1.4 T, ≈ 0.7 K), for the smaller cross section, and only of one point (2.8 T, 0.9 K) for the greater one.

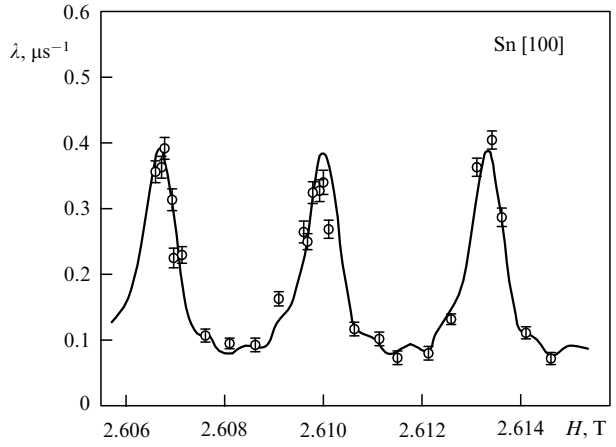

Figure 11. $\lambda(H)$ dependence with increasing H in the 2.6 T region. Solid curve depicts the result of calculations for the second (greater) cross section with $F_2 = 2080$ T corresponding in the given field to the period $\Delta H = 33.3$ G.

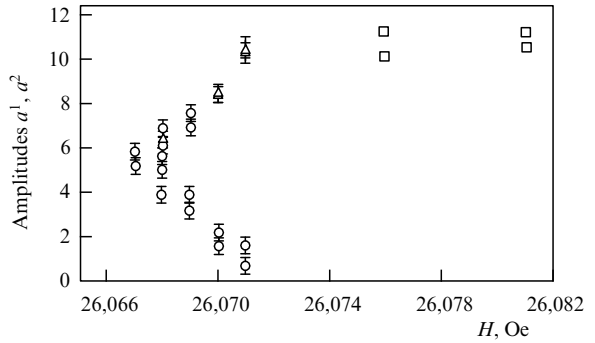

Figure 13. Variation of amplitudes a^1 (curves) and a^2 (triangles) for dia- and paramagnetic phases in the domain region near $H = 26{,}070$ Oe (see Fig. 12). Squares mark the homogeneous phase.

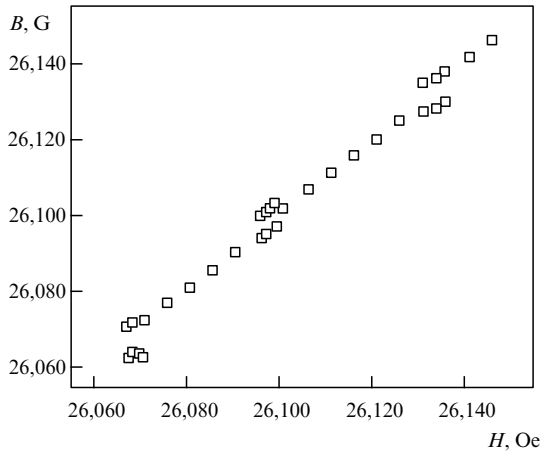

Figure 12. Induction B as a function of the applied field strength H for the same field range as in Fig. 11. Periodic formation of Condon domains with the splitting $\Delta B \approx 8$ G is observed. Characteristically, the domain part exhibits sloping plateaus instead of the usual horizontal ones.

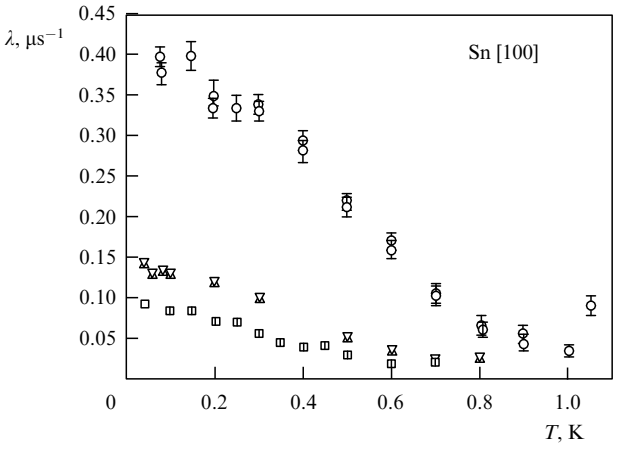

Figure 14. Decrease in the damping constant $\lambda_{\max} \propto \Delta B$ with increasing temperature for both cross sections. Circles correspond to the cross section F_2 in magnetic field $H = 2.6$ T. Squares stand for the cross section F_1 at $H = 1$ T, and triangles at $H = 1.4$ T.

2.3.2 Aluminium, lead, and indium. Similar studies were carried out on aluminium, lead, and indium. All these metals have Fermi surfaces with the cross sections suitable for measurements with an LTF spectrometer. In all samples, oscillations of λ with the 'correct' period were obtained (as mentioned in Section 2.3.1), which definitively suggests the diamagnetic domain formation in these metals. However, no doublet structure was identified, and domains disappeared at a temperature of around 0.5 K.

Aluminium contains Fermi surfaces in the 3rd Brillouin zone with the well-known [55] electronic sheets resembling deformed rings with the fourth-order symmetry (ring arms), which were positioned opposite quadrilateral faces of the truncated octahedron in the 2nd zone. The maximum dHvA signal occurs at $\mathbf{H} \,||\, (100)$. In this case, four cross sections of a single ring 'work' simultaneously. However, any uncontrolled small-angle deflection from this direction (as likely as not during sample mounting in a given experiment) inevitably leads to appearing beats with an unpredictable period. Therefore, we chose direction $\mathbf{H} \,||\, (110)$ at which the respective cylindrical pieces of the Fermi surface are parallel and only one frequency is present. Such a sample, $17 \times 12 \times 1.4$ mm in size, was measured over a range of magnetic fields from 1 to 2.8 T.

Well-apparent oscillations of $\lambda(H)$ with the amplitude $\lambda_{\max} = 0.18\ \mu s^{-1}$ were already obtained at $H \approx 1$ T and $T = 0.02$ K against the background of $\lambda \approx 0.06\ \mu s^{-1}$ corresponding to the homogeneous phase. The period $\Delta H = 35.5 \pm 1$ G corresponds to magnetic frequency $F = H^2/\Delta H \approx (282 \pm 8)$ T, which practically coincides with the well-known value of $F_{\gamma 5} = (287 \pm 1)$ T for this cross section [55]. The value of $\lambda_{\max} = 0.18\ \mu s^{-1}$ is appropriate to the splitting $\Delta B \approx 4$ G that is too small for the given resolution, as discussed in Section 2.3.1. The situation does not change qualitatively under variations of magnetic field up to ≈ 1.5 T, and the continuous domain formation is accompanied by peak splitting too small for resolution.

Measurements on a $17 \times 12 \times 0.15$-mm lead sample with $\mathbf{H} \,||\, (110)$ showed that λ oscillations appear only in the strongest fields. Their period corresponds to the cross section of a multiply connected electronic Fermi surface in the 3rd zone. At $T = 0.02$ K and a magnetic field of 2.4 T, the value of $\lambda_{\max} = 0.18\ \mu s^{-1}$ is the same as in aluminium and corresponds to the splitting $\Delta B \sim 4$ G against a somewhat higher baseline value of $\lambda \approx 0.08\ \mu s^{-1}$ for the homogeneous phase. The oscillation period $\Delta H = 34 \pm 0.5$ G is appropriate to the magnetic frequency $F = (1693 \pm 25)$ T consistent to an accuracy of 5% with the well-known experimental frequency $F_\zeta = 1809$ T [56, 57]. The minor discrepancy can be accounted for by an inaccuracy in sample orientation. Here, as in the previous case, the anticipated splitting $\Delta B \sim 4$ G is too small to detect a doublet.

The indium lattice is structurally close to that of aluminium but shows slight 'tetragonality' in the direction (100). As a result, interstitial sites in indium, where muons reside and travel, are nonequivalent. It significantly slowers muon diffusion in indium compared to that in aluminium. In indium, a muon very soon gets trapped in the most suitable interstitial site, whereas in aluminium it rapidly moves over equivalent interstitial sites. Then, randomly oriented nuclear fields undergo averaging, which accounts for a relatively small value of $\lambda = 0.06\ \mu s^{-1}$ in the state with homogeneous magnetization. In indium, the level of λ in the homogeneous state is much higher and domain formation leads to not quite pronounced $\lambda(H)$ oscillations in the field region around 2 T. In all metals, λ ceases to oscillate at $T \approx 0.5$ K.

To conclude, the use of the μSR method for the study of diamagnetic domains proved very fruitful. It may be stated now that Condon domains are not at all an exotic phenomenon but form in all metals. For any extremal belt of a metal there are appropriate magnetic field and temperature ranges where Condon domains have to appear provided the quality of crystals is sufficiently high.

Unfortunately, the μSR method provides no information about domain structure. It permits, in principle, determining the dimension of domain walls, but this possibility needs a higher resolving power to be realized. The feasible, and highly probable, structure of diamagnetic domains can be deduced from comparison with the intermediate state of a type-I superconductor, well-characterized in the recent past. Despite the essential difference in the nature of the two phenomena, they share the property of separating into two phases, i.e., Condon domains or superconducting and normal phases. In both cases, the cause behind the phase separation is the sample geometry. Indeed, a plate normal to the field cannot pass stepwise from one state to another, as in a long sample with an almost zero demagnetization factor, i.e., from B_1 to B_2 or from $B = 0$ to $B = H_c$. The minimum energy corresponds to the separation of the plate state into these two phases [58, 59]. Quantitative estimates show that many equally thick samples contain structures of a similar size.

The intermediate state was investigated by a variety of experimental methods, including decoration with magnetic powders and magneto-optic technique that was employed to most advantage [59, 60]. Also, muons were used to study intermediate states in tin and aluminium [61, 62]. Unfortunately, these methods are inapplicable to Condon domain research. Magnetic contrast between phases in a superconductor accounts for 100% compared to an order of magnitude with $1/n$ (n is the number of the Landau level) or less in Condon domains. In the most favorable situation (beryllium), the $\Delta B/B$ ratio does not exceed 0.1%. Moreover, the magnetic field itself is two orders of magnitude stronger. This problem was addressed using micro Hall probes, as described in Section 3.

3. Studies of Condon domains by Hall probes

3.1 Description of the method and samples

Obviously, domains can be detected from inhomogeneous induction at the metal surface. Thus, Meshkovskii and Shal'nikov [63] were the first to reveal and study induction homogeneity in the intermediate state of tin. Condon has already tried to realize this idea by moving a magnetoresistive sensor over a beryllium surface. An analogous attempt was made by us earlier on beryllium as well using a Hall probe with an active area of $\approx 40 \times 40$ μm. Such probes have an important advantage over magnetoresistive sensors due to much higher (almost field-independent) real sensitivity and much lower resistance.

However, no inhomogeneity in excess of approximately 1–2 G was found in the sample despite a noise level of ≈ 1 G, sufficiently low temperature (≈ 1.4 K), and field range of up to 6 T at which $\Delta B \approx 100$ G could be expected. At the same time, there were no doubts as regards domain formation in this sample because it had been used earlier to measure μSR as described in Section 2, and the presence of domains was

definitively confirmed by observation of magnetic breakdown oscillations of thermopower and resistance. Relying on these evidences, it was concluded that the size of the domains was much smaller than expected (~ 100 μm) and that thin-film Hall probes need to be used [64, 65].

The experimental device was manufactured at the Max Planck Institute for Metals Research, Stuttgart (MPG–Germany) by the molecular epitaxy technique with subsequent optical lithography; all measurements were taken at the Grenoble High Magnetic Field Laboratory (CNRS–France). A sandwich was grown on a crystalline GaAs substrate. A 1-μm-thick silicon-doped GaAs layer (with a carrier concentration of around 4.3×10^{16} cm^{-3} at $T = 4.2$ K, and mobility of about 2000 cm^2 V^{-1} s^{-1}) was placed between 10-nm-thick undoped GaAs layers. Contacts for 10 Hall probes were connected to 24 bonding sites that were attached to the measuring system by spot welding. The resolving power of the probes was higher than 1 G.

Figure 15 presents a magnified schematic drawing of the experimental layout. This geometry was expected to be more or less suitable at a domain structure period p ranging from 10 to 100 μm. The sample was homogeneously magnetized in the diamagnetic phase of the dHvA period and all probes gave identical voltages. At least one of the sensor systems ought to have recorded nonuniform distribution of induction in the case of domain formation in the paramagnetic phase of the dHvA period. Oblong samples were chosen in which the laminae were supposed to be stretched across the sample.

The operating capacity of this device was tested using a magnetic structure that arose in the intermediate state of a type-I superconductor and had characteristics similar to those expected in Condon domains. The sensors recorded the anticipated stepwise changes of induction in a properly sized sample of pure tin upon a very slow variation of the magnetic field (0.1 G s^{-1}) in the intermediate state range. The jumps coincided in some probes, but not in others. Outside this range, probe readings evidenced either 0 or external field values. This sample and all the others were glued by narrow strips of cigarette paper to fix them relative to the Hall probes, and were slightly pressed to the probe-carrying substrate by a cotton pad and a light spring from beryllium bronze to ensure a close contact.

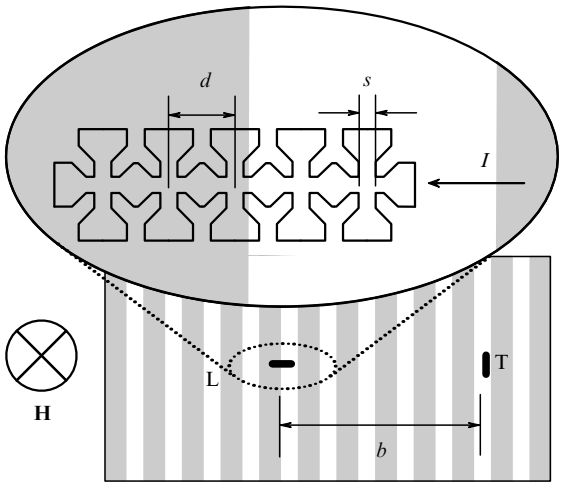

Figure 15. Longitudinal (L) and transverse (T) arrays of Hall probes on the sample. A hypothetical domain structure is shown by black and white stripes. Distance between the L- and T-arrays is $b = 1$ mm, and between the probes is $d = 40$ μm; each Hall probe possesses an active area of $s = 10$ μm.

The test specimens were oblong plates with a demagnetization factor of 0.5. They were mounted above the Hall probes so that their longitudinal array was arranged along the longest sample side. Beryllium samples ($4.5 \times 1 \times 0.8$ mm) and plates for μSR measurements were cut out from the same crystal by electrospark erosion method. The hexagonal axis of the crystal was normal to the larger side. Resistance ratio reached $R_{300\,\mathrm{K}}/R_{4.2\,\mathrm{K}} \approx 300$. Dingle temperature $T_\mathrm{D} = 2$ K was estimated from dHvA oscillations.

Silver samples were prepared by V A Gasparov exactly as described in Refs [66, 67]. The domain structure was studied using a sample measuring $2 \times 1.6 \times 1.0$ mm with the axis (100) normal to the longest side. Ratio $R_{300\,\mathrm{K}}/R_{4.2\,\mathrm{K}} \approx 16{,}000$ had been measured earlier by the contactless Zernov–Sharvin method [68]. The high quality of the crystal accounted for the extremely low Dingle temperature $T_\mathrm{D} \leqslant 0.2$ K (taking account of all errors in the measurement of the dHvA amplitude [69]).

The samples were polished with a fine-grit diamond paste to make their surface ideally flat and mirror-like.[2] As is known, this procedure leaves defects in a crystal at a depth by an order of magnitude greater than the paste grit size. Therefore, we used a series of diamond pastes, with the last one having a grit size of about 0.1 μm.

3.2 Measurements in silver and beryllium

Measurements were made in a superconducting magnet with a field of up to 10 T. Field homogeneity in the center of the solenoid in the sphere 1 cm in diameter was estimated at 10^{-5}. A stable source of electric current ensured maintenance of a constant magnetic field to an accuracy of $\approx 10^{-6}$. The sample-containing insert was placed in a separate cryostat, the tail of which remained in the warm bore of the large cryostat. A water-cooled copper solenoid between the cryostats was employed to vary the main magnetic field in the range $H_\mathrm{v} = \pm 15$ mT with a single period as long as a few hours. The temperature in the inner cryostat could be lowered to 1.3 K by pumping out helium. A constant current (100 μA) passed through the Hall probes and their voltages were read out simultaneously by five Keithley voltmeters. The correct calibration of the Hall probe was tested in the range 4.2–3.6 K where the sample was homogeneously magnetized and all probes gave identical voltages. Periodic splitting of the readings in both probe arrays was for the first time noticed in silver at low temperatures. Figure 16 illustrates typical $B(H)$ dependences for the 1st and 5th probes of the L-array at a constant external field $H_\mathrm{ap} = 10$ T.

The observed dependences were reversible upon a change of field scanning direction. The magnetic frequency of examined oscillations exactly corresponded to the maximum Fermi surface cross section ('belly') in silver, mentioned in Condon's experiment. The result of Fourier analysis was consistent with the value of 47,379 T, well known for silver. Maximum splitting δB corresponding to the difference in induction between domains was in excellent agreement with that reported by Condon ($\delta B = 12$ G). The value of δB was measured over a wide range of magnetic fields and temperatures; it made possible extrapolation for determining intersection points in the phase diagram for silver on the plane (H, T): $T \approx 3$ K at $H \approx 10$ T, and $T \approx 1.3$ K at $H \approx 5$ T. These

[2] Thanks are due to J Marcus for assistance in applying this technology.

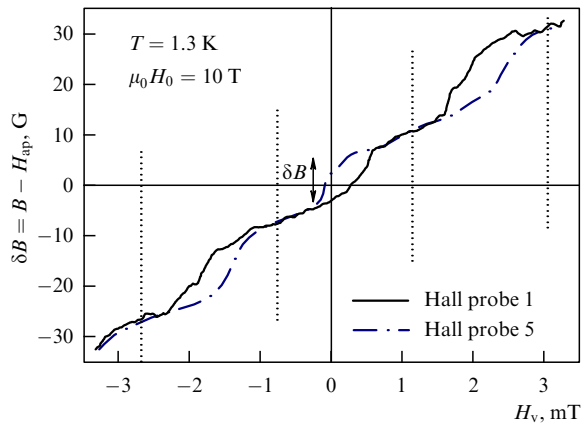

Figure 16. Dependences $\delta B = B(H) - H_{ap}$ for a silver single crystal with $\mathbf{H} \,||\, (100)$ between probes 1 and 5 of the L-array over a range of three dHvA periods separated by vertical dotted lines.

results fairly well agree with the phase diagram in silver calculated by using the LK formula with the Dingle temperature of 0.2 K as a parameter [71, 72]. Excellent agreement between all the results obtained in silver experiments and calculations in the framework of LK theory can be naturally accounted for by the almost spherical shape of the Fermi surface, as mentioned earlier in Ref. [69].

Variation of the magnetic field in the domain state range leads to a change in the volume of dia- and paramagnetic phases and in the displacement of domain boundaries. The sequence of transitions from one phase to another for adjacent probes can be used to determine the direction in which the boundary moves. Comparison of transition sequences in L- and T-arrays of probes reveals a significant difference. Figure 17 gives an example of phase transitions in the T-array.

It is easy to see that the extreme Hall probes 1 and 5 are the first, and the 3rd (central) probe is the last to undergo transitions. The same, but in the reversed order, takes place in the case of the opposite field scanning direction. Therefore, it is natural to conclude that the domain boundary is slightly curved in this case and passes most likely across the sample. Comparison of many T-transitions reveals their highly chaotic order.

The picture was totally different when the probes were aligned along the sample. It is clear from general considerations that the orientation of domain boundaries across the sample is advantageous in that it makes them shorter. Such an orientation is inherent in the L-array. The sequence of transitions is always either *1–2–3–4–5* or the reverse. Although domains evidently tended to align across the sample, as expected, their structure remained somewhat chaotic: it was only natural to try to put it in order. We used the idea of Yu V Sharvin first realized in studies on the structure of the Sn intermediate state [59, 60]. He tilted a tin disk at a small angle ($\approx 20^\circ$) and thereby turned the formerly chaotic structure into a regular laminar one oriented along the tilt; it was possible because the domain walls tended to be directed parallel to the magnetic field.

In our case, the sample was pressed to the substrate and the entire assembly had to be tilted relative to the sample's long axis. The tilt angle was chosen to be 13°. There was only one cross section of the Fermi surface ('belly') in this magnetic field direction. In contrast, a whole set of cross sections revealed themselves in previous measurements at $\mathbf{H} \,||\, (100)$ [8], which led to amplitude beats. Figure 18 exemplifies phase transitions in a tilted sample under the same conditions (1.3 K, 10 T) as in Fig. 17.

The order of transitions in Fig. 18 is strictly constant over the entire field range; the resultant structure can be regarded as a laminar one aligned strictly across the sample. The existence region of domains in each period is slightly narrowed due to reduction of the magnetization factor in the tilted sample.

Analysis of experimental findings leads to several conclusions regarding domain structure characteristics in silver.

(1) There is never more than one transition from one phase to another over the whole array of Hall probes during a single dHvA period. This means that there is never more than one boundary between dia- and paramagnetic phases over a length of the entire array. Therefore, period p of the domain structure is at least as long as a length of this array. It may be assumed that $p \geqslant 150$ μm.

(2) Transitions from one phase to another in each Hall probe are rather sharp compared with the region in which the domain state exists, meaning that domain wall thickness w is much smaller than domain structure period, i.e., $w \ll p$.

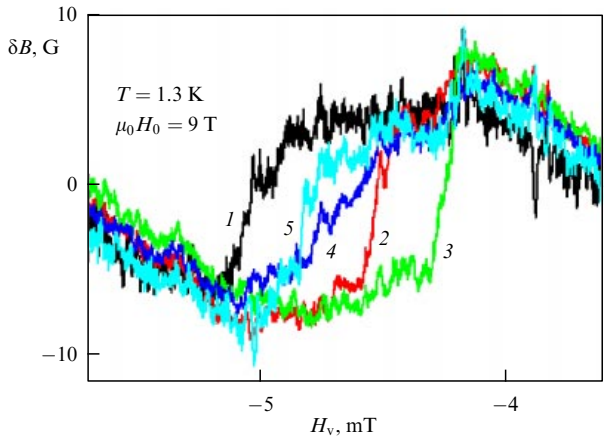

Figure 17. Example of successive transitions of five T-probes between dia- and paramagnetic phases. The applied field was swept at about 0.5 mT min^{-1}.

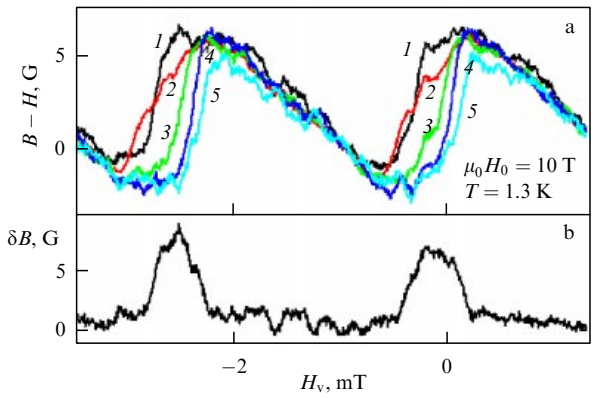

Figure 18. (a) Example of transitions between dia- and paramagnetic phases in L-array probes for a sample tilted 13° at $T = 1.3$ K, and $H = 10$ T. Transition order is *1–2–3–4–5* or the reverse if the field is swept in the opposite direction. (b) Maximum value of $\delta B = B_1 - B_5$.

(3) The distance between two neighboring probes (the probe size being 10 μm) in the L-array is 40 μm; in other words, the gap between them is around 30 μm. Very often such probes show different intermediate readings in transitions from one phase to another. This means that the boundary thickness is comparable with the interboundary gap size and the estimate $w = 20$ μm may be regarded as its lower limit.

Using the known relationship between domain structure period p, sample thickness t, and domain wall thickness w, i.e., the formula

$$p \sim (wt)^{1/2},$$

one may estimate the domain structure period. At $t = 1$ mm and w on the order of a cyclotron radius [11–13] that equals 1 μm in a magnetic field of 10 T in silver, one finds $p \sim 30$ μm, as in Ref. [14]. This value is at least 5 times smaller than the lower limit for p deduced from our measurements. Therefore, the accepted estimate $w \geqslant 20$ μm is quite consistent with the estimated period.

Thus, the transverse dimensions of the silver domain structure in a magnetic field of 10 T ($p \geqslant 150$ μm and $w \geqslant 20$ μm) proved much bigger than expected ($p \sim 30$ μm, $w \sim 1$ μm). This means that measurement quality can be improved by using much thinner silver samples or a different geometric arrangement of the Hall probes for samples with a given thickness.

In principle, there is one more way mentioned in Section 3.1, namely, moving a Hall probe relative to the sample. Displacement of domains inside the sample cannot be excluded, either. If a small transverse gradient superimposed on a homogeneous magnetic field does not distort the homogeneity necessary for domain formation, a gradual variation of the external magnetic field will cause the periodically emerging domain structure to move along the sample. Generally speaking, such domain structure can move as a whole (as in the intermediate state of superconductors, see Ref. [59]). In this case, measurements with a single Hall probe can, in principle, give exhaustive information about the domain structure, i.e., its profile.

Another scenario is equally feasible. A domain structure can behave like an expanding forest in which new trees grow at one edge, while old ones die at the other. In this way, the forest expands even if individual trees remain stationary. In this case, a chain of probes is needed to gather information about the domain structure; such a system was actually used.

Beryllium experiments preceded silver ones. The ΔB amplitude was naturally expected to be largest in beryllium. A sample cut out of the same crystal as the plate was utilized, in which domains with ΔB over 40 G in a magnetic field of 2 T were detected by the μSR method. The splitting was anticipated to be $\Delta B \sim 100$ G in magnetic fields of 3.6–4.8 T (in oscillation amplitude antinodes). However, thorough long-term experimentation with such a sample failed to yield a positive result.

It may seem odd because domain formation was indirectly confirmed in independent experiments on magnetic breakdown oscillations of resistance and thermopower, mentioned in Section 1.3. The beryllium sample was polished exactly as the silver one even though the procedure took much more time, the material being harder. Therefore, there is no doubt the quality of the polished beryllium surface was as good as that of silver. Still, nothing was found except minor induction inhomogeneities on the sample surface (not exceeding 1.5–2 G). Probably, 'traces' of the domain structure on the beryllium surface will be discovered using a measuring method with a higher resolving power. However, it will not change the main conclusion ensuing from our experiment, namely that Condon domains exist only in the bulk of beryllium samples. This fact appears to account for the failure of all previous beryllium experiments, including those with the application of the NMR method [14]. It should be emphasized that this important, even if negative, result was possible to ascertain only after successful silver experiments.

Thus, it is safe to say that virtually unaltered Condon domains come out to the crystal surface in some metals (e.g., silver) and form only in the bulk of others (at least in beryllium). In the former case, their structure is similar to that in the intermediate state of type-I superconductors, while in the latter case the domain structure remains to be elucidated. Maybe this difference can be understood taking into account magnetostriction and the elastic properties of metals.

4. Relationship between magnetostriction and Condon domains

4.1 The mechanism of magnetization current

The origin of the dHvA effect is considered in both Landau and Lifshits–Kosevich theories only from the thermodynamic point of view; in other words, the magnetic moment oscillating in a magnetic field is just a result of the oscillatory contribution to the electron energy during formation of quantum Landau levels. This concept disregards the mechanism of emergence of orbital magnetization current. The problem of orbital magnetization in metals (or, to be precise, its absence in an ordinary situation) has long been a subject of discussion, although it is actually nonexistent from the energetic standpoint because the magnetic field in classical physics does not change electron energy and there is no magnetic moment. Nevertheless, the enormous diamagnetic moment due to electrons in diamagnetic Larmor orbits needs to be compensated. Evidently, such compensation can be ensured only by the motion of electrons near the surface of the metal (at distances smaller than the Larmor orbit diameter).

This problem is discussed at greater length in the book by R Peierls [73] by the example of a potential box in which electrons in Larmor orbits create diamagnetic current and hopping electrons bounced from the surface generate paramagnetic current. It is argued in Ref. [73] that these currents are identical and that the proof of the relevant theorem is given in Niels Bohr's lectures [74]. Unfortunately, attempts to find the proof of interest were foiled [75]. It is therefore appropriate to offer the proof we arrived at earlier in Ref. [10] using a simple model of electron motion in Peierls' potential box (see Appendix). The proof itself is not as interesting as the conditions under which compensation takes place. To begin with, the size of the box is much bigger than that of the electron orbit; second, electrons are uniformly spread inside the box (as a rule, due to electroneutrality); third, the orbit size is much bigger than the distance between electrons. The last condition is equivalent to a limitation on the magnetic field strength that must be below the ultraquantum limit.

The picture is different in the case of the dHvA effect. There is an oscillating magnetic moment which implies periodic disturbances of compensation. At first site, this is

not surprising because the metal passes into a state with an energy minimum and the problem of the recompensation mechanism fades into insignificance. Nevertheless, it was considered in some detail by Teller [76], who categorized all electrons into two groups: bulk electrons moving rather far from the boundary, and surface ones. Integrating over all states in the framework of the Fermi surface spherical model, Teller obtained the general expression for magnetization current. Certainly, the total current broke up into two, J_b and J_s, generated by bulk and surface electrons, respectively, and described by different expressions. It can be concluded from general considerations (see the book [77] by F Bloch for details) that the two currents must compensate for each other in classical mechanics. However, the expression for J_b changes when bulk electron motion gets quantized. The expression for J_s remains unaltered since surface electrons are not subjected to quantization (mirror reflection from the surface was not considered). Generally speaking, compensation becomes impossible. This difference determines the magnitude of magnetization. Recently, the contributions of bulk and surface electrons to magnetization have been comprehensively analyzed by V P Mineev. Specifically, it was shown that the main contribution to the dHvA effect is made by bulk electrons, whereas both contributions are essential in Landau diamagnetism [78, 79].

This issue is thoroughly discussed here because magnetization current running in the domain wall during diamagnetic domain formation cannot be described in terms of the above mechanism. Indeed, hopping orbits characteristic of surface electrons inside or on either side of the domain wall are out of the question because the wall is located in the ideal-quality single crystal and electrons everywhere move along circular orbits. A small magnetic field gradient at the domain boundary, associated with the arising domain structure, may create a low drift current along the boundary but it flows in the opposite direction. Therefore, this current only shields the domain structure.

Thus, there is no choice but to recognize that the sole remaining cause behind the appearance of magnetization current is the electron density gradient in the magnetic field [80]. (To recall, we are dealing here with simple metals and orbital magnetization, which excludes consideration of electron spin.) As a rule, electron density in metals, unlike that in plasmas, is to a high accuracy constant due to electroneutrality, and such currents are absent. (A rare, if not the sole, exception is the situation described earlier in Ref. [81].) However, the electron density gradient may arise from a small lattice deformation that does not affect electroneutrality. Generally speaking, such small deformation of the domain wall must result from reverse magnetostriction in neighboring dia- and paramagnetic phases. It was therefore interesting to study and measure magnetostriction in the presence of diamagnetic domains [82, 83].

4.2 Magnetostriction and diamagnetic domains in beryllium

Magnetostriction in metals, including nonmagnetic ones, has been known for a long time. The earliest experiments using bismuth were reported by P Kapitza [84] in 1932 already. Chandrasekhar [85] was the first to notice in 1963 that magnetization oscillations (the dHvA effect) are always accompanied by magnetostriction oscillations. During the short period that followed, experiments on magnetostriction oscillations in Ag, As, Bi, Cd, Cu, Ga, Sb, Sn, and Zn [86], and beryllium samples of different orientations [87] were performed. All of them used samples with a demagnetization factor smaller than unity, as is usual in dHvA measurements. Therefore, no diamagnetic domains formed in these experiments.

The aim of our work [81] was to study magnetostriction under conditions suitable for diamagnetic domain formation. It was done using the same single-crystalline beryllium sample in which domains had been observed to form earlier by the μSR method (see Section 2.2). In addition, formation of the domain structure in this sample was established, as before, from observations of magnetic breakdown oscillations of thermopower.

We measured magnetostriction ε in a plate, i.e., oscillations $\delta l = \varepsilon l$ of the longest side ($l = 1.1$ cm) of the sample. It was placed in a capacitance dilatometer where changes in the size of the test sample resulted in a change in the capacity of the plane capacitor. The movable spring-controlled plate of the capacitor had a pointed protrusion that leaned against the sample edge (Fig. 19). The adjusting screw on the opposite side of the sample was used to slightly move it and thereby alter the gap between the capacitor plates and the initial capacity of the capacitor. The adjustment could be made only at room temperature. With lowering temperature, the gap between the capacitor plates decreased due to different expansion coefficients of the sample and the holder frame. It was therefore necessary to exercise caution during the control in order to rule out the shorting between the capacitor plates and to ensure that the final capacity was slightly lower than 100 pF at helium temperature, in accordance with the maximum resolving power of the bridge.

The sample was installed in the center of the superconducting solenoid, whose magnetic field homogeneity within the sample was not worse than $\pm 0.015\%$, i.e., inhomogeneity was always significantly smaller than 1/10 of the period. The magnetic field was normal to the plane of the plate and parallel to the sample hexagonal axis. Measure-

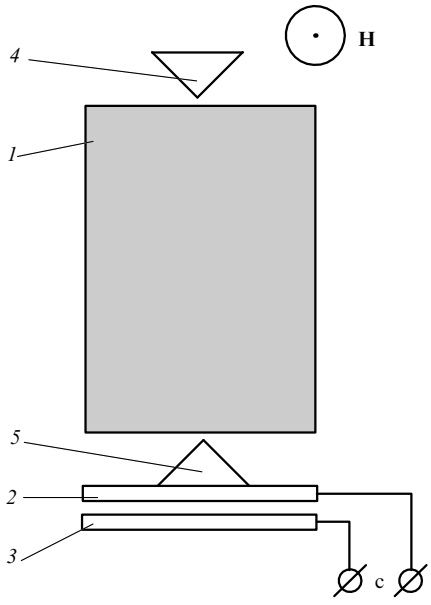

Figure 19. Schematic of a dilatometer that houses a sample: *1* — beryllium single crystal (9 × 11 mm), *2* — movable capacitor plate (the spring is not shown), *3* — stationary capacitor plate, *4* — adjusting screw, 5 — pointed protrusion of movable capacitor plate, c — measuring bridge input.

ments were made in helium (both normal and superfluid) or its vapors, the results being significantly different in terms of noise level and character. In the normal liquid, the noise due to helium boiling reached roughly 2×10^{-3} pF. It decreased in superfluid helium, but sudden measured capacity outliers occurred from time to time. Moreover, the passage of the liquid-helium level through the capacitor was accompanied by a strong capacity drift which made measurement practically impossible. Helium vapor at $T = 1.5$ K was the most favorable medium for this purpose: the noise was only $\approx 0.5 \times 10^{-3}$ pF, corresponding to the relative deformation of the sample $\varepsilon \equiv \delta l/l \approx 5 \times 10^{-9}$. The temperature was monitored from the vapor pressure. The capacity was measured using a semi-automatic Tesla BM484 bridge, to which the capacitor was connected with shielded wires, thus excluding the effect of their capacity on the results of measurement [88].

Magnetostriction was measured in 10–70 kOe fields at helium temperatures. The dependences of magnetostriction on the external magnetic field at $T = 4.2$ K were almost identical in shape with oscillations of the magnetic moment with beats characteristic of beryllium. At the same time, a more complicated signal was recorded over the field range from 20 to 60 kOe at 1.5 K, i.e., in the conditions and field range at which diamagnetic domains formed in the sample. At the beginning, small amplitude dips near sample size maxima appeared, which became deeper as the magnetic field strengthened. In the field range from 39 to 42 kOe, the 'dips' compared with the oscillation amplitude, so that the frequency of oscillations seemed to double (Fig. 20a). Oscillations acquired the form of usual magnetic moment oscillations as the field continued to increase starting from $H \approx 60$ kOe, i.e., on disappearance of the domain structure .

Such unusual behavior was naturally ascribed to the formation of diamagnetic domains. It was suggested that the formation of a domain structure — a peculiar state with two concurrently existing phases (in the general case, of different densities) — may be accompanied by a significant decrease in the compressibility coefficient. As a result, the existing tips, namely the pointed protrusion on the movable capacitor plate and the adjusting screw end (*4* and *5* in Fig. 19) abutting against the sample's surface with a minimal force (just to keep it in place) periodically slightly 'came down' into the sample. (Notice that beryllium is a hard metal, being inferior only to iridium and tungsten as far as this property is concerned). This experimentally established effect was possible to prevent by putting ≈ 0.1-mm-thick copper spacers under the copper tips. Figure 20 compares results of the measurements with and without the spacers in the same magnetic field range and under similar conditions.

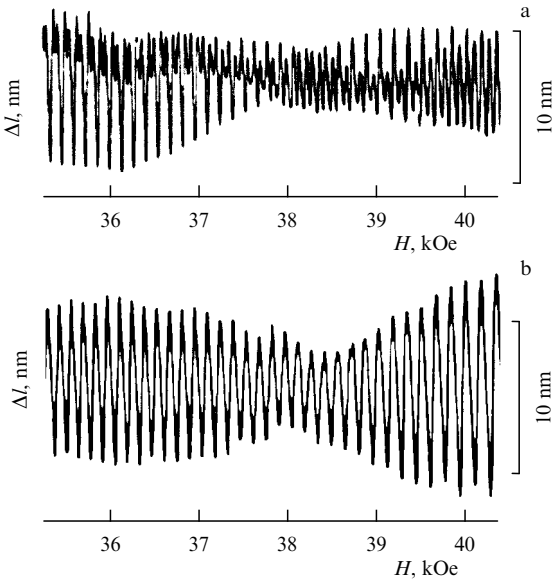

Figure 20. Comparative results of magnetostriction measurements without copper spacers (a) (see Fig. 19) and with the spacers (b) under identical experimental conditions.

Experiments with the use of protective copper spacers revealed a clearly delineated sawtooth signal, the amplitude of which markedly increased in the field range where diamagnetic domains formed. Ascending and descending portions of the 'saw' alternatively corresponded to the homogeneous state with a gradually varying size of the sample and to the two-phase state consisting of oppositely deformed dia- and paramagnetic domains in which size and magnetization variations were due to periodic changes in the phase volume ratio. The oppositely deformed phases were associated with different charge, electron and hole densities accounting for the emergence of magnetization current in the domain wall. It should be noted that oscillation amplitude from one peak to another was practically unaltered in magnetic fields down to 30 kOe [82].

It follows from the above that 'pits' under the tips should be interpreted as resulting from the enormous enhancement of compressibility during diamagnetic domain formation [82]. A domain structure being properly a mixture of two phases of different densities, such a local rise in compressibility ('hypersoftness') is not at all surprising. Opposite deformation of dia- and paramagnetic domains matches their different densities. Therefore, formation of the pits can be regarded as a result of the partial rearrangement of the domain structure near the tips where the pressure is higher and greater phase density is more advantageous.

4.3 The role of deformation in domain initiation

Let us discuss at greater length the role of deformation in domain initiation. Consider the expression for energy variation $\delta\Omega$ in a magnetic field, taking into account the energy of magnetization and the energy of deformation:

$$\delta\Omega = a\cos\varphi + \frac{1}{8\pi}(B - H)^2 + \frac{1}{2}E(\varepsilon_x^2 + \varepsilon_y^2 + \varepsilon_z^2)\,. \quad (15)$$

For beryllium, formula (15) provides a good approximation because the anisotropy of its compressibility coefficient is very low, $\pm 5\%$ [89], and the Poisson coefficient is almost zero; therefore, all deformations may be considered mutually independent. From this standpoint, beryllium is a unique metal with Young's modulus $E = 300$ GPa and the compressibility coefficient $K = -V^{-1}\partial V/\partial P = 9.97 \times 10^{-12}$ Pa^{-1} [90]. The well-known relation $K^{-1} = E/[3(1 - 2\sigma)]$ gives the Poisson coefficient $\sigma = 5 \times 10^{-3} \approx 0$, in excellent agreement with the known tabulated data [90]. Under thermodynamic equilibrium conditions, one has

$$\frac{\partial\Omega}{\partial\varepsilon_i} = 0\,, \quad i = x, y, z\,, \quad (16)$$

whence it follows that

$$\frac{\partial\Omega}{\partial\varepsilon_i} = -a\sin\varphi\,\frac{\partial\varphi}{\partial\varepsilon_i} + \varepsilon_i E = -a\varphi\sin\varphi\,\frac{1}{F}\frac{\partial F}{\partial\varepsilon_i} + \varepsilon_i E = 0, \quad (17)$$

and the expression for striction takes the form

$$\varepsilon_i = \frac{a\varphi}{E}\,\frac{1}{F}\,\frac{\partial F}{\partial \varepsilon_i}\sin\varphi\,. \tag{18}$$

By differentiating $\widetilde{\Omega} = a\cos\varphi$ with respect to B, one can write

$$-M = \frac{\partial \widetilde{\Omega}}{\partial B} = a\varphi\,\frac{1}{B}\sin\varphi\,, \tag{19}$$

which, in comparison with formula (18), yields the well-known relation [8] establishing the proportionality between striction and magnetization:

$$\varepsilon_i = \frac{-MH}{E}\,\frac{1}{F}\,\frac{\partial F}{\partial \varepsilon_i}\,. \tag{20}$$

Equation (20) contains H instead of B because the difference between them is insignificant: $B - H = 4\pi M \ll H$. (This difference needs to be taken into account only for a phase change within the period.) Expressions for striction in other directions can be derived in a similar way. As a result, magnetization of a crystal (in this case, along the z-axis) is accompanied by its deformation in all directions; generally speaking, this anisotropic deformation is needed for a change in δF. Since all deformations are very small, these quantities, including δF as well, may be regarded as linearly interconnected. This means that an energy change (15) in a magnetic field can be represented as a function of two variables: induction B, and deformation δF (a result of striction). The external magnetic field H plays the role of a parameter.

Figure 21 shows schematically a 'three-dimensional' plot in the form of a paraboloid with the apex at the point $(H, 0)$, which is superimposed with a ripple image $\widetilde{\Omega} = a\cos\varphi$ caused by the Landau levels and proportional to a. To recall, a is determined by experimental conditions (temperature, magnetic field) and sample quality (Dingle temperature).

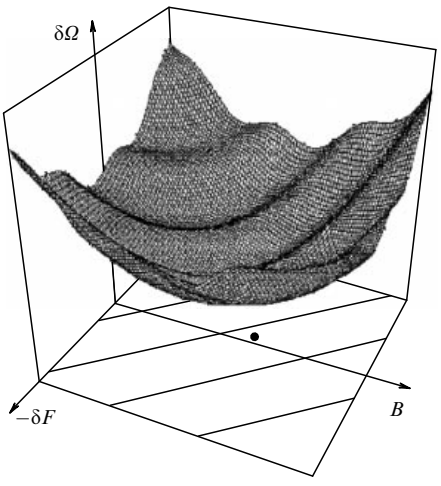

Figure 21. Schematic representation of energy changes $\delta\Omega$ depending on induction B and δF proportional to the sample deformation at a given external magnetic field H. The slant straight lines in the plane $(B, \delta F)$ correspond to constant phase values $\varphi = 2\pi F/B$, where the energy $\widetilde{\Omega} = a\cos\varphi$ is minimal. The point in the plane $(B, \delta F)$ shows the position of the projection of the absolute energy minimum slightly shifted leftward and upward with respect to the paraboloid apex $(H, 0)$. With a change in H, this minimum 'depicts' the phase trajectory of simultaneous deformation and magnetic moment oscillations, shown in Fig. 22.

Clearly, the ripple causes displacement of the minimum on plane $(B, \delta F)$ with respect to the apex $(H, 0)$. A leftward and upward shifts, i.e., to the state with $B < H$ and $\delta F > 0$, correspond to a transition into the diamagnetic state upon sample deformation with an increase in the cross section F and, accordingly, charge density N. Rightward and downward displacements in the second half of the period correspond to a transition to the paramagnetic state with $B > H$, a negative change in δF, and lower N. In accordance with formula (20), the relationship between these displacements, i.e., the deformation-to-magnetization ratio within the period, is constant with high accuracy. In other words, the tilt angle of phase displacement is directly proportional to the magnetic field, and inversely proportional to Young's modulus (20).

The slant lines in the plane $(B, \delta F)$ (Fig. 21), corresponding to constant phase values, are depicted in Fig. 22 for two of them, viz. $\varphi_n = 2\pi n$ and $\varphi_{n-1} = 2\pi(n-1)$. Curve a_1 (or a_2) is the 'trace' of the energy minimum position, i.e., the phase trajectory of the simultaneously magnetized and deformed state of a metal during variation of the external magnetic field. At a small ripple amplitude a_1, this trajectory remains continuous everywhere (see Fig. 22). However, the state of the metal becomes unstable when the amplitude of a_2 is large enough (i.e., condition $4\pi\chi \geqslant 1$ is practically met) and the position of H is exactly in the center of the period, where oscillatory contribution $\widetilde{\Omega} = a\cos\varphi$ has a maximum (here, the Landau level is half-filled). The value of $\delta\Omega$ at point 1 becomes equal to $\delta\Omega$ at point 2, meaning that at a demagnetization factor close to zero (as in a thin rod aligned along the field) the entire sample passes jumpwise from state 1 to state 2 with a change in both deformation and magnetization (the Shoenberg effect) in the opposite direction. If the demagnetization factor is close to unity (as in a plate normal to the field), the plate state in the region $B_1 \leqslant H \leqslant B_2$ undergoes separation into phases 1 and 2 or B_1 and B_2, differing in both deformation and magnetization. Naturally, magnetization and deformation (as well as electron densities N_1 and N_2) within each phase are constant. However, a smooth transition from state 1 to 2 must take place near the interphase (interdomain) boundary, i.e., deformation and electron density must change in the domain

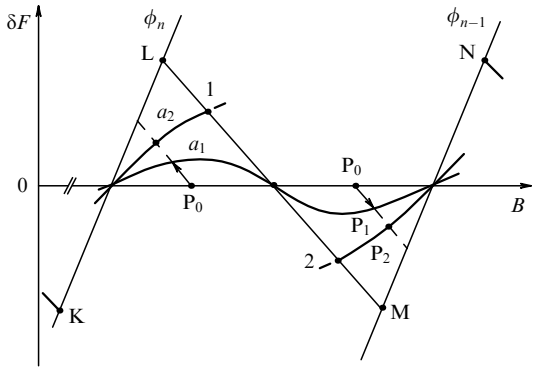

Figure 22. Phase trajectories of the metal state. Slant lines φ_n and φ_{n-1} correspond to constant phase values $\varphi_n = 2\pi n$ and $\varphi_{n-1} = 2\pi(n-1)$ at which oscillatory contribution $\widetilde{\Omega} = a\cos\varphi$ has a minimum. Curves a_1 and a_2 are phase trajectories at different ripple amplitudes ($a_1 < a_2$). Trajectory a_1 is continuous, and transition between points 1 and 2 in the trajectory a_2 occurs with a jump. Points P_1 and P_2 show a change of state with respect to point P_0, viz. $(H, 0)$. KLMN follows the phase trajectory of a quasi-two-dimensional electron gas.

wall. The difference between electron densities in states 1 and 2 creates a charge density gradient in the domain wall and, accordingly, magnetization current in the magnetic field traversing the domain wall and responsible for difference $\delta B = 4\pi\delta M$ between neighboring domains.

There is every reason to think that the same mechanism of formation of magnetization current operates in the case of homogeneous magnetization when the sample contains no domains. Then, striction is uniform over the entire sample except a near-boundary region where closed Larmor motion of electrons is impossible at distances from the boundary smaller than the Larmor diameter, the corresponding oscillatory contribution to the energy is absent, deformation vanishes, and the resulting difference in charge densities creates magnetization current.

Doubtless, deformation is isotropic in a homogeneous (dia- or paramagnetic) phase. The same appears to be true of the deformation that develops during the emergence of 'new' phase domains as long as this phase is so small that it consists most likely of separate inclusions. As the new phase grows in volume, it must 'rapidly' acquire the energetically more preferred laminar structure. A good example is the behavior of 'domains' in the intermediate state of a type-I superconductor [62, 91], where isolated thread-like inclusions occur only in a state very close to the transition to a normal one.

In the case of a laminar structure, we cannot regard each phase as locally isotropic because the difference between deformations in neighboring domains 'accumulates' along the interphase boundary, thus leading to shear stress and enhanced energy. In this context, it is much more advantageous to realize the necessary difference in electron densities by deformation normal to the boundary. In a laminar domain structure, therefore, anisotropic deformation is possible in separate domains, but the structure of the entire crystal must remain, on average, isotropic (unless there is a preferential direction) by virtue of a mosaic orientation of laminar portions, as in a similar situation in the intermediate state [91].

Anyway, there remains some difference in deformations of neighboring domains along the magnetic field. This fact leads to the conclusion that domain wall thickness cannot but enhance with increasing the thickness of the crystal. This inference is in conflict with the suggestion that the thickness of the domain wall is on the order of the Larmor diameter, as in the Privorotskii theory [11–13]. Probably, the Larmor diameter plays the role of the lower limit of domain wall thickness for thin samples.

4.4 Relationship between magnetization current and deformation

As mentioned in Section 4.1, magnetization current in the domain wall may be due to the charge density gradient. In what follows, we shall compare the difference in magnetizations of neighboring domains, i.e., magnetization current, with their deformations resulting from magnetostriction, i.e., with the corresponding change in electron density in the diamagnetic wall. The experimentally found magnetization difference and magnetostriction in neighboring domains are used here for quantitative comparison.

The formula for magnetization current density in a magnetic wall was derived in Ref. [80]:

$$\mathbf{j}_{\mathrm{m}} = c\,\mathrm{rot}\sum_k n_k(\mathbf{r})\,\boldsymbol{\mu}_k\,. \tag{21}$$

Here, $n_k(\mathbf{r})$ is the number of Larmor orbits corresponding to magnetic moment $\boldsymbol{\mu}_k$ per unit volume. Integrating expression (21) over domain wall thickness from one domain to another for our purpose and taking into account that orbital magnetic moments of all electrons are parallel to the external magnetic field, we obtain magnetization current in the domain wall per unit length along the field:

$$J = c\sum_k (N_2 - N_1)_k\,\mu_k\,, \tag{22}$$

where $(N_{1,2})_k$ are the bulk densities of charges with the magnetic moment μ_k in neighboring domains. The difference δN being extremely small, all orbits may be regarded as residing on the Fermi surface. Characteristic quantities may be estimated as follows. Magnetic moment of the Larmor orbit is given by

$$\mu = \frac{J_0 S}{c}\,,$$

where

$$J_0 = \frac{e\omega_{\mathrm{c}}}{2\pi}\,,\quad S = \pi R_H^2\,,\quad R_H = \frac{v_\perp}{\omega_{\mathrm{c}}}\,.$$

Here, ω_{c} is the cyclotron frequency, e is the electron charge, R_H is the Larmor radius, and $v_\perp$ is the velocity of an electron at the Fermi surface normal to the field direction. Then, the total current J in the domain wall per unit length in the direction of the magnetic field is defined as

$$J = \frac{\delta N e}{2}\,\overline{\omega_{\mathrm{c}}}\,\overline{R_H^2}\,, \tag{23}$$

where δN is the total difference between the numbers of charge carriers (electrons and holes) in neighboring domains, i.e., the difference between volumes under the Fermi surface in these domains, and $\overline{\omega_{\mathrm{c}}}$, $\overline{R_H^2}$ are the corresponding quantities averaged over this surface.

Since beryllium is a compensated metal, the volume of electrons in the 3rd Brillouin zone (two cigars) and that of holes in the 2nd zone (coronet) are always identical. Therefore, δN can be found from a change in the cigar volume alone, which simplifies calculations because the shape of the cigar is close to that of a cylinder. For the total difference between Fermi surface volumes in neighboring domains, one obtains

$$\delta N \approx N_0\left(\frac{\Delta F}{F} + \frac{\Delta L}{L}\right) = N_0\sum_i\left(\frac{1}{F}\frac{\partial F}{\partial\varepsilon_i} + \frac{1}{L}\frac{\partial L}{\partial\varepsilon_i}\right)\varepsilon_i\,. \tag{24}$$

Here, N_0 is the total number of charge carriers (overall volume of the Fermi surface, i.e., two cigars and the coronet) in beryllium, and quantities in parentheses characterize relative changes in the cigar volume in opposite domains as a result of total deformation (F and L are the cigar's cross section and length, respectively). Quantities $(\partial F/\partial\varepsilon_i)/F$ and $(\partial L/\partial\varepsilon_i)/L$ are easy to determine from the well-known relationship between the Fermi surface and the size of the Brillouin zone in beryllium [39, 92–94]. This is especially true as far as beryllium is concerned, whose Poisson coefficient $\sigma \approx 0$ and all deformations may be regarded as mutually independent (see Section 4.3). Calculations assuming that the cigar is formed by the intersection of three Harrison spheres are in excellent agreement with experiment

[86]; therefore, one arrives at

$$\frac{1}{F}\frac{\partial F}{\partial \varepsilon_{x,y}} = -1\,, \quad \frac{1}{F}\frac{\partial F}{\partial \varepsilon_z} = 6\,, \quad \frac{1}{L}\frac{\partial L}{\partial \varepsilon_{x,y}} = -1\,, \quad \frac{1}{L}\frac{\partial L}{\partial \varepsilon_z} = 1.6\,.$$

By taking deformations $\varepsilon_x = \varepsilon_y = \varepsilon$ and $\varepsilon_z = 6\varepsilon$, we have $\delta N \approx 50\varepsilon N_0$, where ε is the change in $\delta l/l$ from one peak to another. It is clear that the large numerical coefficient equaling 50 is due to the fact that the beryllium Fermi surface formed near the corners and edges of the Brillouin zone makes up only a small part of the Harrison sphere. (Naturally, this coefficient is 3 in a free-electron model.) The values of ω_c and R_H in the basal plane for a cigar are well known: $\omega_c = eH/(m^*c) = 4.17 \times 10^{12}\ \mathrm{s}^{-1}$, $m^* = 0.16m_e$, $H = 4 \times 10^4$ G, $R_H = v_F/\omega_c = 0.24 \times 10^{-4}$ cm, and Fermi velocity $v_F \approx 10^8$ cm s^{-1}. The total number of charge carriers in conformity with the available data [39] is 0.01573 electrons per atom, with two atoms per unit cell, cell volume is 109.0758 a.u.^{3}, and the number of holes equal to the number of electrons; hence, $N_0 = 0.43 \times 10^{22}$ cm^{-3}. Notice that the latter value is 1.6% of the Harrison sphere volume.

To sufficient accuracy, the half-area of the cigar's central orbit can serve as a measure of the mean orbit area πR_H^2. Then, taking together all the above estimates, substituting them into formula (23), and using for δN the known value of $\varepsilon \approx 1.37 \times 10^{-6}$ (Fig. 20b) in field $H = 4 \times 10^4$ G, we find $J \approx 29$ A cm^{-1}, in satisfactory agreement with $\Delta B = 4\pi\Delta M \approx 40$ G (Fig. 9a) observed in work [42], despite the rough estimates used and slightly different conditions of both experiments.

The expression (23) for current can be rewritten as

$$J = f_1 \delta N \varepsilon_F \frac{c}{H}\,,$$

where the coefficient f_1 takes account of orbit averaging over the Fermi surface. Because the induction jump in neighboring domains is defined as $\Delta B = 4\pi\Delta M \equiv (4\pi/c)\,J$, one obtains immediately that

$$\Delta M H = f_1 \delta N \varepsilon_F\,,$$

where it may always be considered that $\delta N = N_0 \varepsilon f_2$, and f_2 is a coefficient unambiguously deduced from the shape of the Fermi surface. As shown above, $f_2 = 50$ for beryllium. Hence, one finds that

$$\Delta M H = f_1 \delta N \varepsilon_F = f_1 f_2 N_0 \varepsilon_F \varepsilon\,.$$

Comparing this result with the expression (20) for striction in the form $\varepsilon = (\Delta M H/E) f_3$, where $f_3 = (\partial F/\partial\varepsilon)/F$, we obtain the equation for Young's modulus

$$E = \varepsilon_F N_0 f_1 f_2 f_3\,, \tag{25}$$

where coefficients f_1, f_2, and f_3 are entirely determined by the Fermi surface structure, ε_F is the electron kinetic energy at the Fermi surface, and $\varepsilon_F = \hbar^2 k_F^2/2m$. For example, in the case of beryllium $k_F \approx 1.03$ a.u.$^{-1}$, and $N_0 = 0.43 \times 10^{22}$ cm^{-3} [39]. Substituting a highly probable value of coefficient $f_1 \approx 0.6$ into formula (25), we come to the correct value of Young's modulus for beryllium: $E = 300$ GPa [89]. In other words, we arrive at the conclusion that the Fermi surface determines with high precision not only the electronic but also the elastic properties of a metal. It should be noted that this result is valid within the accuracy of the assumption (correct in itself) that magnetization current entirely depends on the charge density gradient in the magnetic field.

4.5 Compressibility and oscillations of the Fermi level

The conclusion we arrived at the end of the preceding section deserves a more detailed discussion. Of special interest is the question of the contribution of conduction electrons to metal compressibility, which closely relates to oscillations of the Fermi level. The opinions of early authors varied. For example, it was estimated at 60–80% in the theoretical study [95]. In contrast, Ref. [96] totally disregarded ion contribution to compressibility. In fact, all the results in work [96] were obtained on the assumption that the elastic properties of the metal (niobium) are entirely due to conduction electrons.

Metal compressibility proved a central issue in the explanation of experiments on chemical potential oscillations in a magnetic field, predicted earlier [97]. It was dealt with in many other experimental studies [8]. In the first beryllium experiment [98], it seemed natural to expect large-amplitude oscillations, but they were not recorded. This result was accounted for in Ref. [98] by hypothesizing that oscillations of the Fermi level in a magnetic field must be compensated for due to magnetostriction if beryllium compressibility is indeed completely dependent on conduction electrons. We rigorously formulated and proved the adequacy and universality of this inference in a later study [10].

Once again, the problem of oscillations of the Fermi level dates back to the work of M I Kaganov, I M Lifshits, and K D Sinel'nikov [97], in which the magnitude of this effect in a magnetic field was defined as

$$\delta\mu_{KLS}(H) = \frac{\partial\tilde{\varepsilon}(H)}{\partial N}\,,$$

where the energy $\tilde{\varepsilon}(H)$ is the oscillatory contribution described by the exact LK formula, as mentioned in Section 1.2, and N is the electron density. The result in Ref. [97] was obtained for the case of constant density N. In reality, however, magnetostriction alters both the volume and the density $N = N_0/V$, where N_0 is the number of electrons in a crystal of volume V. The overall change in the Fermi level taking account of magnetostriction is given by

$$\mathrm{d}\mu = \delta\mu_{KLS} + \frac{\partial\mu}{\partial V}\,\delta V\,,$$

where δV is the real change in the crystal volume under the effect of striction. Let us represent $\delta\mu_{KLS}$ as

$$\delta\mu_{KLS} = \frac{\partial\tilde{\varepsilon}}{\partial V}\frac{\partial V}{\partial N} = \frac{V}{N}\,\delta\tilde{p}\,,$$

where changes in pressure and volume are

$$\delta\tilde{p} = -\frac{\partial\tilde{\varepsilon}}{\partial V}\,,$$

$$\delta V = \frac{\partial V}{\partial p}\,\delta p^*\,,$$

respectively, and δp^* is the change in the pressure due to striction. The pressure in a sample with a free boundary does not change at all:

$$\delta\tilde{p} + \delta p^* = 0\,,$$

and the complete change in the Fermi level is defined as

$$d\mu = \frac{V}{N}\,\delta\tilde{p}\left(1 + N\,\frac{\partial\mu}{\partial V}\,\beta_{\rm met}\right).$$

Here, $\beta_{\rm met} = (1/V)\,\partial V/\partial p$ is the total compressibility of the metal.

Next, we have the relationship

$$\frac{\partial\mu}{\partial V} = -\frac{\partial p}{\partial N},$$

and simple transformations

$$\frac{\partial N}{\partial p} = -\frac{\partial(N_0/V)}{\partial p} = -\frac{N_0}{V^2}\,\frac{\partial V}{\partial p} = -\frac{N}{V}\,\frac{\partial V}{\partial p} = N\beta_{\rm el},$$

lead to

$$\frac{\partial\mu}{\partial V} = -\frac{1}{N\beta_{\rm el}}.$$

Here, $\beta_{\rm el}$ is the electron gas compressibility that can be found, in principle, from the equation of state for this metal. In other words, $\beta_{\rm el}$ is the compressibility due to electron–electron interaction, i.e., the kinetic energy of the electron gas. Finally, we have for complete displacement of the Fermi level:

$$d\mu = \delta\mu_{\rm KLS}\left(1 - \frac{\beta_{\rm met}}{\beta_{\rm el}}\right).$$

This formula and measurement of contact potential difference permit, in principle, finding $\beta_{\rm el}$. For $\beta_{\rm met} = \beta_{\rm el}$, the contribution to compressibility comes only from the kinetic energy of the electron gas. Then and only then, the effect of Fermi level oscillations is completely compensated for by magnetostriction. Therefore, the absence of Fermi level oscillations does not contradict the result obtained in Ref. [97], where the model of a metal with a constant electron density was considered and striction was totally disregarded.

The supposition that the 'lion's share' of the compressibility coefficient in other metals is also determined by conduction electrons is, generally speaking, confirmed by the theoretical calculations of Brovman and Kagan [99] for the example of magnesium. The contribution of conduction electrons remaining after summation of all electron and ion contributions to compressibility (see Table 3 in Ref. [99]) with an accuracy not worse than $\approx 3\%$ conforms within the same accuracy to the known tabular value of Young's modulus for magnesium.

Thus, conduction electrons must entirely determine the compressibility coefficient of a metal on the assumption that all magnetization current in a domain wall is due to lattice deformation. Nevertheless, it follows from the aforesaid that this inference applies to all metals. Indeed, there is no doubt that diamagnetic domains can form in any metal; the problem is that it is extremely difficult to create the conditions necessary to realize this possibility. As mentioned in preceding sections, diamagnetic domains have already been observed in silver, beryllium, tin, indium, and aluminium. On the other hand, if compressibility of a metal is entirely due to electron contribution, variation of the magnetic field must lead only to oscillations of its volume and magnetization without alteration of chemical potential. This means that there is neither contact potential difference nor 'extra' electrostatic energy between neighboring domains and that Condon domains must form in all metals. In other words, the very fact of their existence confirms that metal compressibility is entirely due to conduction electrons. Nevertheless, a question remains valid what is a precision level of this conclusion.

In the end, the mechanism of emergence of magnetization current is unambiguously related to magnetostriction. Magnetostriction whose amplitude is inversely proportional to Young's modulus is responsible for lattice deformations in metals, which, in turn, cause opposite changes to electron density in neighboring domains. As a result, the charge density gradient in a domain wall generates in a magnetic field the magnetization current necessary for the induction difference to arise between the neighboring phases.

On the other hand, deformation of the crystal lattice in a domain wall results in the appearance of an additional elastic energy. The two states on either side of this boundary correspond to an energy minimum, even though they differ by a finite value as far as the size of their crystal cells is concerned. Because the states of the lattice on either side of the boundary, i.e., the jump-like change in the cell size on the left and right, are given in advance, the excess elastic energy would be lower as the boundary across which this change spreads would be thicker. For this reason, the thickness of the domain wall in large magnetic fields, when the Larmor radius decreases, may be much greater than this radius, as revealed by measurements of the domain structure in silver. Moreover, it suggests the disadvantage of long boundaries because the difference between cell sizes is known to accumulate along the domain boundary. The limitation on the boundary length in the plane of the plate can be obviated by taking advantage of the patchiness of the laminar domain structure. The boundary length along the magnetic field being the sample thickness, there is no alternative but to increase the thickness of the domain wall or to further complicate the structures. In light of the aforesaid, the character of magnetostriction in beryllium can possibly be a cause behind the absence of Condon domains on its surface.

5. Hysteresis and phase diagram of the domain state

The occurrence of the effects of irreversibility in the magnetization processes is attributable to the presence of various defects responsible for energy barriers that arise during the motion of domain boundaries. Hysteresis in usual magnetic materials whose magnetic properties are due to the intrinsic atomic magnetic moment has been the subject of extensive studies [100]. Things are quite different when magnetization results from the orbital motion of electrons in a quantizing magnetic field under the formation of Landau levels. These conditions give rise to an energy oscillating in the magnetic field and to the corresponding magnetic moment created by electron orbital motion, i.e., the dHvA effect. For all that, the energy of the metal remains minimal as the magnetic field varies. It is natural to expect a reversible behavior of magnetization observed in numerous experimental studies [8].

The situation changes radically when diamagnetic domains (Condon domains) are being formed. Indeed, a transition from the state with homogeneous magnetization to that with two phases separated by the domain boundary and having different inductions, opposite deformations, and

magnetization current flowing between them constitutes a first-order phase transition [31]. In this case, it is natural to expect all the phenomena accompanying such a transition, viz. nucleation, hysteresis, and supercooling. Not surprisingly, these issues were discussed in the very first study by Condon [1]. The author failed, however, to observe the above phenomena despite a thorough analysis of all the data available in his time. In a later study [14], Condon and Walstedt noticed a difference in the domain formation when varying the temperature around 2.2 K, which was attributed to supercooling. In subsequent years, these problems remained the focus of attention of both theorists [101] and experimenters.

As mentioned in Section 2.3, we tried to detect hysteresis in muon experiments [42]. We managed to 'almost' see slight irreversibility, i.e., a 1–2 G shift in $\lambda(H)$, when increasing or lowering the magnetic field. On the other hand, no appreciable difference was recorded during similar temperature measurements in a constant magnetic field (see Fig. 12). For this reason, the problem of the existence of hysteresis related to these phenomena remained unresolved; it could only be speculated that the hysteresis was extremely small.

A detailed discussion of the development of instability under condition (9) and domain formation with inductions B_1 (diamagnetic phase) and B_2 (paramagnetic phase) in a plate normal to the magnetic field in the range of $B_1 < H < B_2$ was presented in Section 1.2. In a sample shaped differently than a plate, i.e., having a demagnetization factor $n < 1$, the instability range in which separation into phases B_1 and B_2 still continues narrows accordingly n times. Certainly, the notion of a demagnetization factor is correct only for samples in the form of a three-axial ellipsoid [41]. For samples of other shapes, the demagnetization factor is taken to be equal to that of an ellipsoid inscribed into the sample. Nevertheless, the sample passes from the homogeneous into the two-phase state at the point of developing instability, despite certain field inhomogeneities near the sample's corners and edges. Looking ahead, it should be noted that the boundaries of the phase diagram for the domain state turned out to be identical for samples of different shapes. At the same time, the geometric structure of the domain state for samples of an arbitrary shape substantially different from that of a plate remains unknown. What is clear is that the state of the sample is separated into the same phases with inductions B_1 and B_2, respectively, undergoing opposite deformation in a certain sense under the effect of magnetostriction, and separated by the domain wall. There is little doubt that deformation is uniformly distributed across the domain wall; therefore, magnetization current in the wall is uniformly distributed, too.

In conformity with the above viewpoint, induction in a domain wall varies linearly from B_1 on one side of the wall to B_2 on the other. Induction other than B_1 and B_2 at which the energy falls to a minimum creates an excess energy ε_w in the domain wall. The profile and the maximum amplitude of the dependence $\varepsilon_w(B)$ in the domain wall from $B = B_1$ to $B = B_2$ are easy to obtain, as viewed in Fig. 2:

$$\varepsilon_w = \tilde{\varepsilon}(B) + \frac{(B-H)^2}{8\pi} - \varepsilon_{\min} ,$$

where $\tilde{\varepsilon}(B)$ is the oscillating energy, $(B-H)^2/8\pi$ is the magnetization energy as shown in Fig. 2, and $\varepsilon_{\min}$ is the minimal total energy (5) at points $B = B_1$ and $B = B_2$, i.e., $\varepsilon_w = 0$ at the wall boundaries. Maximum excess energy ε_w in the center, where $B = H_0$, is $\delta\varepsilon$. Let us change the variables:

$$B = H_0 + h$$

and assume that h in the domain wall varies over the range

$$-h_0 \leqslant h \leqslant h_0 ,$$

i.e., let us take the function ε_w as symmetric with respect to point $h = 0$; then, $h_0 = (B_2 - B_1)/2 = \Delta B/2$. Such an assumption is quite in order at large numbers of the Landau level, as is always the case in the presence of domains. Then (see Fig. 2), $\varepsilon_w(h)$ in this range can be presented with a high precision in the form

$$\varepsilon_w(h) = \frac{\delta\varepsilon}{2}\cos\frac{\pi h}{h_0} + \frac{\delta\varepsilon}{2} .$$

As a result, we have for the second derivative

$$\frac{\partial^2\varepsilon_w(h)}{\partial h^2} = -\frac{\delta\varepsilon}{2}\left(\frac{\pi}{h_0}\right)^2\cos\frac{\pi h}{h_0} \approx \frac{\partial^2\tilde{\varepsilon}(B)}{\partial B^2} + \frac{1}{8\pi}\frac{\partial^2(B-H)^2}{\partial B^2} = -\chi + \frac{1}{4\pi} .$$

In other words, the maximum value of the excess energy $\delta\varepsilon$ is given by

$$\delta\varepsilon = \frac{2h_0^2}{4\pi}(4\pi\chi - 1) = \frac{(\Delta B)^2}{8\pi^3}(4\pi\chi - 1) .$$

It is appropriate to compare this result with the theory [11–13], where the energy proportional to

$$(B_1 - B_2)^2 - (2B - B_1 - B_2)^2$$

was taken as the excess energy in the domain wall; this energy also vanishes at the boundaries of this range, and the maximum excess energy per unit volume equals

$$\varepsilon_w(0) = \frac{(\Delta B)^2}{4\pi} .$$

Thus, the real excess energy profile (see Fig. 2) is significantly different from the theoretical one [11–13], not only quantitatively due to the presence of an additional multiplier $2\pi^2$ in the denominator but also qualitatively since it has a different shape (its derivative with respect to a coordinate vanishes at the range boundaries).

As a result, the surface energy in a domain wall must be at least 40 times lower than in Refs [11–13]. On the other hand, the thickness of the domain wall is usually much greater than the Larmor radius due to additional elastic energy (see Section 3.2). Therefore, such large thickness must prevent domain wall pinning at lattice point defects during wall movements. The aforesaid may account for the very small hysteresis, i.e., weak coercive force.

5.1 Experiment

We first discovered hysteresis in dHvA effect during diamagnetic domain formation in beryllium [102]. It was actually very small (below 2 G or two orders of magnitude smaller than the dHvA period). The beryllium sample was a parallelepiped $8 \times 2 \times 1$ mm in size, with the long side

parallel to the hexagonal axis. The sample was cut out from the same crystal as the remaining ones, including a plate in which Condon domains were detected using muon spectroscopy. Moreover, the sample exhibited the presence of magnetic breakdown oscillation envelopes characteristic of the domain state and described in Section 1.3. In other words, there was no doubt regarding the formation of diamagnetic domains in this sample. The sample's Dingle temperature was 2 K. Induction in the sample was measured by a Hall microprobe placed right up to the sample's end.

We do not discuss here how the induction measured at the end differs from that in the center of the sample. This issue was touched upon earlier in paper [40]. Notice only that the two values are practically identical for type-I superconductors residing in the superconducting state with $B = 0$. The same seems to be nearly true of our beryllium sample, although it does not actually matter too much.

Far more important is the fact that the superconducting solenoid had its own hysteresis due to the diamagnetism of its winding [103]. For this reason, the external magnetic field was measured by another Hall probe positioned rather far from the sample (ca. 1 mm or the distance between L- and T-arrays in Fig. 15).

Figure 23 shows the results of direct measurement of magnetic induction $B(H)$ by a Hall probe when increasing and reducing the magnetic field.

It can be seen that hysteresis is very small and noticeable only in a magnified view. The result was obtained at a very slow sweep rate, ensuring a signal-to-noise ratio on the order of 10. It should be emphasized that the data presented in Fig. 23 were obtained under very favorable conditions for such measurements, i.e., at a very low temperature and in the region around a dHvA antinode. A similar result is difficult to obtain at other temperatures and in other magnetic field regions, and practically impossible close to the boundary of the region where diamagnetic domains exist. In other words, direct measurement by dc Hall probe technique is not sensitive enough and cannot be used for detailed studies of hysteresis in the entire (H, T) region.

A method with modulation of the external magnetic field proved much more sensitive for the detection of arising domains. It is the standard ac modulation technique in which the sample is placed in one of the two pickup coils, and the decompensation signal proportional to the sample's magnetic susceptibility at a rather small external field modulation amplitude is measured with a lock-in amplifier. As a rule, the modulation amplitude h was chosen to be at least two orders of magnitude smaller than the oscillation period, and a low modulation frequency (21 Hz) was used.

Measurements were made with the solenoid utilized in previous experiments. This method allowed precise detection of the transition point from homogeneous magnetization to instability origin and diamagnetic domain formation. It turned out that setting the modulation amplitude much smaller than it appears necessary from a comparison with the dHvA period ensures a reliable observation of two phases. Usually, the signal being measured corresponded with high accuracy to magnetic susceptibility $\chi(H) = \partial M/\partial H$ if the modulation amplitude was much smaller (e.g., by an order of magnitude) than the period. A further decrease in the modulation amplitude led to a proportional decrease in the signal amplitude; however, the normalized signal value (related to the modulation amplitude) tended to a limit, viz. $\chi(H)$, and did not change any more. Specifically such measurements were made using a beryllium sample in the same fields as in Fig. 23. The period was higher than 150 G, and modulation $h \approx 6$ G gave a limiting value of the normalized signal. It seemed that a further decrease in modulation amplitude should not have any effect, probably excepting a change in the signal-to-noise ratio. However, it proved otherwise.

As illustrated in Fig. 24, measurements with modulation amplitude $h = 6.2$ G and those by a Hall probe without modulation yielded in the truth the same susceptibility values. In the case of an even smaller modulation ($h = 0.5$ G), the result was altogether different.

The signal did not change in the vicinity of nodes where the oscillation amplitude was three times smaller than in antinodes, in conformity with the correctly measured average slope of the magnetization curve. Also, plots for the diamagnetic part of the dHvA period ideally coincide (coincidence takes place in all parts of the magnetic field

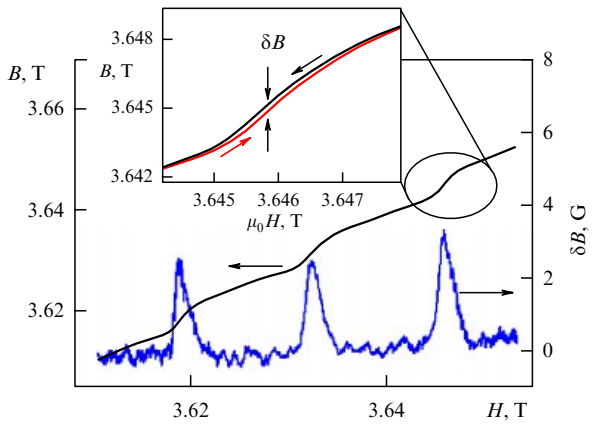

Figure 23. $B(H)$ dependences measured by Hall probes for an up and down sweep of the applied magnetic field around a dHvA amplitude antinode at 1.3 T (left-hand scale). The inset depicts a magnified hysteresis loop observed in the paramagnetic component of each period. The induction difference δB between these curves shown in the lower part of the figure characterizes the value of hysteresis (right-hand scale).

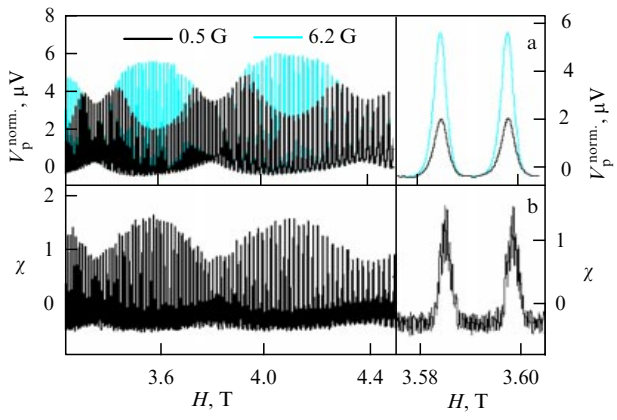

Figure 24. (a) Normalized pickup voltages divided by different modulation levels for modulation amplitudes 6.2 G (grey) and 0.5 G (black) at 1.3 K. (b) Susceptibility $4\pi\chi$ derived from magnetization measurements with Hall probes (without field modulation). Graphs in the right panel show respective zooms of the field region corresponding to an oscillation antinode.

with the wittingly homogeneous magnetization state). The coincidence disappears for the components of the dHvA period showing paramagnetic susceptibility, as soon as the susceptibility amplitude reaches the value of $4\pi|\chi| \geqslant 1$. From this instant on (Fig. 24a), the signal amplitude begins to decrease rather than increase and becomes much smaller than expected. A simple assessment shows that this decrease is actually related to the formation of a two-phase state exactly at the point where the correct amplitude starts to fall. Of course, such a curtailed amplitude no longer corresponds to the average slope of $M(H)$ or real susceptibility. The amplitude notch effect completely disappears at temperatures above ≈ 3.5 K, where Condon domains are absent.

That the amplitude notch effect results in faulty measurement of susceptibility is easy to check in the following way. The integral of susceptibility must conform to oscillations of the magnetic moment about a certain mean value that is, generally speaking, close to zero. It is exactly such a situation that takes place everywhere at a high temperature in the absence of domains or in the vicinity of nodes when they are present only in antinodes. But as soon as the notch effect manifests itself, magnetic moment oscillations sharply decrease, i.e., the mean value drops dramatically, which cannot actually happen.

Such seemingly strange behavior can be accounted for by the magnetization irreversibility, i.e., hysteresis, that arises during transition to the two-phase state. As mentioned above, hysteresis remains small even when it reaches a maximum far from the phase boundary. The more so it is small in a region close to the phase transition, where its magnitude tends to zero. In the case of modulation amplitude $h \approx 6$ G, which is much smaller than the dHvA period but essentially greater than the magnitude of hysteresis, measurements yield a more or less correct average slope estimate. However, when small modulation amplitude h compares with the hysteresis magnitude or, more exactly, with its coercive force, the result is altogether different.

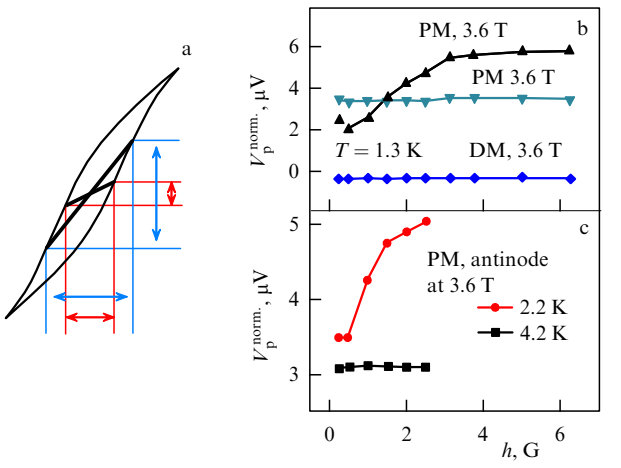

Figure 25. (a) Schematic representation of the hysteresis loop showing that the normalized response to a decrease in modulation amplitude is nonlinear. (b) Modulation amplitude (h) dependence of the normalized pickup voltage (average subloop slope) in different parts of the magnetic field at 1.3 K: at an antinode (normal triangles), and a node (inverted triangles); both dependences pertain to the paramagnetic (PM) phase of the dHvA period; rhombi show the dependence for the case when the phase is diamagnetic (DM) throughout. (c) The same dependence for an antinode at $T = 2.2$ K and $T = 4.2$ K; marked nonlinearity arises at $T \approx 3.1$ K.

This line of reasoning is schematically illustrated in Fig. 25a. As soon as modulation amplitude becomes on the order of hysteresis (coercive force) or smaller, the magnetization subloop is found entirely inside the complete hysteresis loop. Then, the average slope of this part of the loop becomes much smaller than the 'right' slope [100]. Such a sharp decrease in 'susceptibility' can be followed up as a function of modulation amplitude over a wide range of temperatures and magnetic fields within the beat half-period, i.e., from nodes to antinodes. The results of such measurements are presented in Fig. 25 b, c.

Figure 25a helps to clarify the origin of the amplitude cutoff effect during the appearance of hysteresis. The curve slope does not change in the diamagnetic phase or in the oscillation node region where there is no room for instability; it is apparent only in the paramagnetic phase and only at low temperatures. The slope begins to sharply decrease at a modulation amplitude $h \approx 2$ G. This value may be regarded as the hysteresis width or the coercive force. In a magnetic field of roughly 3.6 T, the above nonlinearity begins to manifest itself at $T \approx 3.1$ K, and the point (3.6 T, 3.1 K) can be taken for the intersection point of the phase boundary of the two-phase state, in agreement with the data obtained by the μSR method.

The explanation of the amplitude cutoff effect as a consequence of the transition to magnetization irreversibility, i.e., the appearance of hysteresis, was validated in a simple way as follows. In routine measurements with the application of the ac modulation technique (as in our experiments), the external magnetic field sweep rate is very low compared with the rate of modulation field variations. In other words, the total magnetic field $H + h$ always oscillates around a given slowly changing field H. Therefore, a 'backward' change in this field in the case of irreversible magnetization always brings back point $B(H + h)$ inside the hysteresis loop, and $B(H + h)$ describes the subloop. If the experimental conditions are modified so as to make $\mathrm{d}h/\mathrm{d}t$ equal to $\mathrm{d}H/\mathrm{d}t$ in absolute magnitude, point $H + h$ will always move 'forward' or stop. In other words, the magnetic field moves only along the hysteresis boundary and never goes back inside the loop. In this case, there is no cause for the irreversible behavior of magnetization. Certainly, such a regime is never used in real ac modulation measurements because the results would be wittingly quantitatively false. Nonetheless, the qualitative result obtained is beyond question. Measurements taken by the above method revealed neither nonlinearity nor the amplitude cutoff effect. They invariably yielded a 'right' picture of beats characteristic of beryllium, which once again confirms the point of view expressed above.

The phenomena described in the preceding paragraphs associated with the occurrence of instability and hysteresis permit explaining here the strange result reported by Plummer and Gordon [104], who used the same modulation method to measure the susceptibility of beryllium over approximately the same field and temperature ranges as in our experiments. Plummer and Gordon interpreted their observation of deep cutoff in the oscillation amplitudes as the appearance of a new magnetic frequency, i.e., a 'new' cross section of the Fermi surface. Certainly, it was a mistake because the beryllium Fermi surface had already been fairly well known. Unfortunately, further discussion of this strange result ended in the wrong conclusion that it was due to eddy currents induced in the sample by the modulation signal [105, 106]. We verified this conclusion by varying the modulation

frequency and found that the cutoff effect remained unaltered.

Investigations of the above effects, especially when they are just starting to emerge, under changes of temperature or magnetic field may provide a basis for the detection of the boundary of the domain state region on the (H, T) coordinates. This approach is certainly more sensitive to the appearance of the two-phase state than all others described here, viz. analysis of magnetic breakdown trajectory envelopes, NMR, peak splitting in muon experiments, and direct observation of $B(H)$ using a Hall probe. It will be shown below that the appearance of hysteresis provides a possibility of determining with a much higher accuracy the onset point of two-phase state formation, i.e., the point of intersection of the phase diagram boundary in relation to both the field and temperature.

The fact is that the cutoff effect in susceptibility amplitude, i.e., attenuation of the first-harmonic signal, is accompanied by a peculiar 'compensation' (a sharp rise in higher-harmonic amplitudes and phase shift of the measured response signal relative to the modulation field). This means that the origin of hysteresis renders the response to a harmonic signal of magnetic field modulation strongly nonlinear and phase-shifted, i.e., delays the response with respect to modulation. This lag is manifested as the sudden emergence of the imaginary constituent in the response.

Figure 26 presents results of the measurement of the 3rd harmonic (Fig. 26a) and the imaginary constituent (Fig. 26b) of the response signal over a wide range of magnetic fields at a temperature of 1.3 K. In both cases, the signal amplitude grows sharply only in oscillation antinodes and only in the paramagnetic phase of each dHvA period, i.e., when hysteresis appears. The signal amplitude is close to zero at other

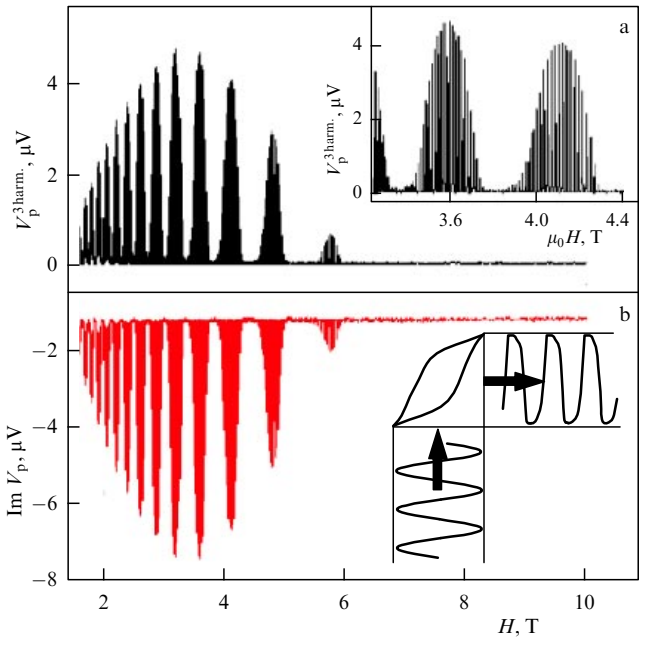

Figure 26. (a) Third harmonic of the pickup voltage; the inset shows a zoom of the same field region as in Fig. 24. (b) Imaginary part of the response ($\pi/2$-shifted signal) produced by coils. In both cases, $T = 1.3$ K, and modulation amplitude is 2.5 G. Inset on the right-hand side of figure (b) schematically depicting hysteresis shows that the response to a sinusoidal field modulation becomes window-shaped, slightly phase-shifted, and delayed with respect to the modulation signal.

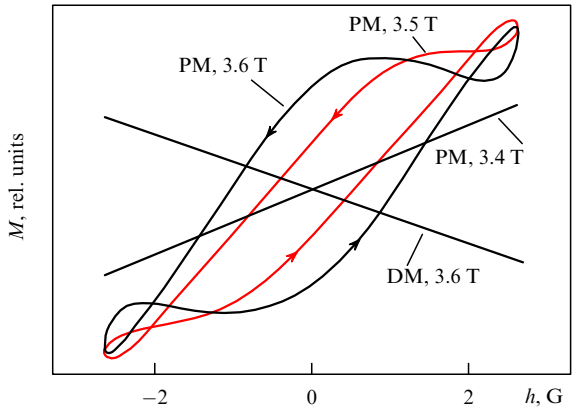

Figure 27. Hysteresis shape reconstructed for a modulation amplitude of 2.5 G at $T = 1.3$ K from the analysis of five harmonics. Reversible and irreversible (hysteresis) magnetization M at different magnetic field values: 3.6 T corresponds to the oscillation antinode region, 3.4 T to the oscillation node, and 3.5 T to the intermediate region.

field values, i.e., in the node region and throughout the diamagnetic phase of the dHvA period.

The inset to Fig. 26a is a magnified view of the 3rd-harmonic signal exactly in the same magnetic field region as in Fig. 24. Comparison of the two readings shows that the signal originates and fades out at the same points of the magnetic field. The two processes proceed in a threshold manner at the point of phase transition to the two-phase state.

The inset on the right-hand side of Fig. 26b demonstrates schematically how hysteresis promotes not only the 'cutoff' effect resulting from the nonlinear decrease in the response amplitude but also a radical change in the shape of the response signal which acquires a window shape. It is equivalent to both the phase shift (delay) and the enhancement of the contribution from odd harmonics, which is characteristic of a meander. This accounts for such a sharp rise in the 3rd-harmonic amplitude upon transition to the two-phase state with hysteresis. In the absence of hysteresis, this amplitude is negligibly low because the modulation amplitude h is small compared with the dHvA period (2.5 and 130 G, respectively, at $H = 3.6$ T in Fig. 26).

The shape and the size of the hysteresis loop can be restored in a standard way using the method described in Ref. [107]. An example is presented in Fig. 27. The response to sinusoidal modulation with an amplitude of 2.5 G was found by summation of all harmonics up to and including the 5th one. Certainly, both real and imaginary components of the receiving signal were summed up. This procedure was performed in different ranges of magnetic field variations.

As shown in Fig. 27, five harmonics are sufficient to qualitatively and even quantitatively represent real hysteresis, barring minor distortions at the boundaries of the modulation range. Hysteresis is absent in the region of node $H \approx 3.4$ T, where instability does not develop either at the given temperature. Certainly, there is no instability in the diamagnetic part of the dHvA period at any magnetic field strength. Hysteresis appears only in the region of antinode $H = 3.6$ T and reaches a maximum in its center.

5.2 Determination of phase diagrams in beryllium and silver

As mentioned in Section 5.1, transition to the two-phase state and the appearance of hysteresis result in a marked enhance-

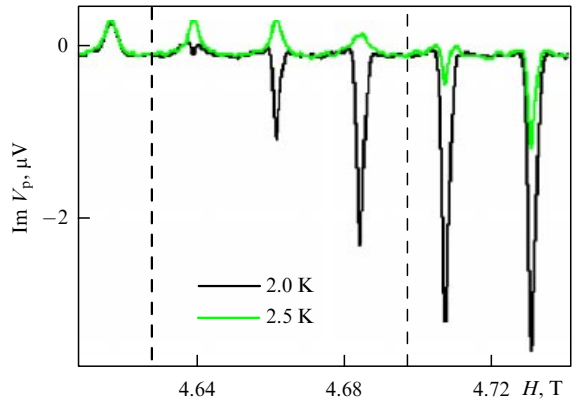

Figure 28. Magnetic field dependences of the imaginary part of the 1st-harmonic signal in beryllium measured at 2.0 K (dark curve) and 2.5 K (light curve) with a 0.4-G modulation amplitude. The sharp rise in the signal absolute value begins upon intersection of the phase diagram boundary: in the second period at $T = 2.0$ K, in the fifth one at $T = 2.5$ K. Dashed vertical lines show the approximate (to within one period) position of the phase boundary for these temperatures (4.63 and 4.69 T, respectively), suggesting an error of ±100 G in the determination of the phase transition point or ≈ 1% of the entire domain region size (see Fig. 30).

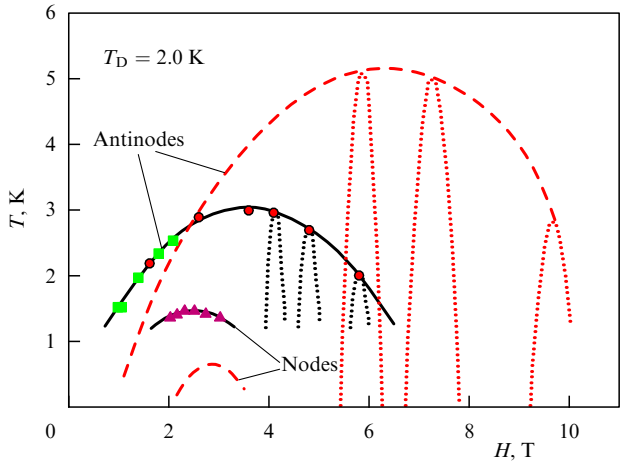

Figure 30. Phase diagram in the (H, T) plane for beryllium with $T_D = 2.0$ K. Solid curves: experimental phase boundary for beat node and antinode envelopes. Circles (antinodes) and triangles (nodes) were obtained when varying temperature in a constant magnetic field, and squares (antinodes) when varying the magnetic field at a constant temperature. For comparison, dashed curves show calculated data [36, 112]. Dotted curves indicate the phase boundary of individual antinodes.

ment of the strongly nonlinear response when either the 3rd harmonic or the $\pi/2$-shifted signal has a clear-cut threshold character. This fact permits determining the point of transition from the homogeneous to the two-phase state with a maximally possible accuracy, for instance, to within one dHvA period (Fig. 28).

This effect disappears at temperatures above 3.0 K, when only weak dHvA oscillations can be observed. It confirms that $T = 3.6$ K is the topmost point of the phase diagram for antinodes. In the region of the phase diagram maximum, however, intersection of the phase boundary in a 'vertical direction', i.e., as temperature varies and magnetic field remains constant, appears to be a more accurate option. Then, the magnetic field is located right in the center of the paramagnetic part of the dHvA period where instability develops (Fig. 29).

It follows from Fig. 29 that hysteresis arises rather abruptly in either dependence, which suggests the possibility

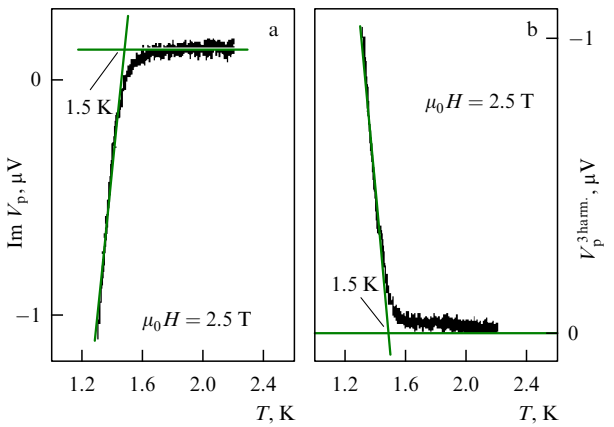

Figure 29. Temperature dependences of the imaginary part (a) and the 3rd harmonic (b) of the pickup voltage in the beat node in the magnetic field of 2.5 T right in the middle of the paramagnetic part of the dHvA period with a 0.4-G modulation amplitude.

of equally well determining the intersection of the phase diagram in both ways. The two dependences exhibit a sharp rise in the signal absolute value (down for the imaginary component, and up for the 3rd harmonic) at the same temperature $T = 1.5$ K. It is in this way that intersection points of the phase boundary in beat nodes were found (see Fig. 30 below).

Also important is the fact that the threshold effect of signal initiation occurs over the wide ranges of frequency (80–200 Hz) and modulation amplitude variations (on the condition that $h \ll \Delta H$, where ΔH is the dHvA period) at the same point in the (H, T) plane. Therefore, the described effect, undoubtedly, can be used to detect Condon domains in the simplest possible way and to most accurately determine the phase diagram under experimental conditions. This approach was employed to show that the position of the phase boundary point does not depend on the sample shape; this observation was verified in special experiments with beryllium plates normal to the magnetic field.

Thus, the origin of hysteresis is associated with the window-shaped signal of response to a sinusoidal modulation magnetic field. Simultaneously, odd harmonics (first and foremost, the 3rd one) sharply increase and a delay (i.e., the imaginary component) appears in the response signal. An analysis of several contributions to the response signal allows the size and the shape of hysteresis loop to be reconstructed. Also, the coercive force can be found from the nonlinear dependence of the response amplitude on the modulation amplitude (see Fig. 25).

The quantitative investigation of hysteresis is of great importance although, it being very small, researchers encounter serious difficulties. Generally speaking, there is no doubt that hysteresis is in one way or another related to the character of domain wall motion and the height of the energy barrier arising when a new phase forms. Due to this, the dependence of the coercive force on the magnetic field and temperature may be a source of important information about this phenomenon and shed light on the nature of anomalous helicon damping in aluminium [18, 19]. Moreover, compre-

hensive studies of hysteresis may be helpful in the development of a more practical theory, in addition to the existing idealized one [108] disregarding real lattice deformations [81]. The threshold character of the appearance of the imaginary part in the 3rd-harmonic response and the independence of instability developing in the sample from its shape open up the possibility of high-precision determining the point of intersection of the phase diagram boundary for the domain state of this metal with the Dingle temperature characteristic of the study sample. All measurement results are presented in the phase diagram drawn in Fig. 30 [109].

Let us compare experimental and theoretical results. To begin with, it should be noted that the very first measurements using muon spectroscopy showed that calculations using the LK formula grossly underestimate dHvA amplitude and, accordingly, the phase diagram [36, 42]. To recall, the cigar-like electron Fermi surface of beryllium, responsible for the dHvA effect under discussion, has a near-cylindrical shape. It is this fact that accounts for the abnormally high dHvA amplitude and for the incorrect results of calculations based on the LK formula. This formula has the Fermi surface curvature A'' at the extremal cross section belt in the denominator and loses its meaning when this parameter tends to zero. The cigar curvature in beryllium being in fact very small [16, 40] may be a cause behind the discrepancy between experimental and theoretical values of dHvA amplitude and the phase diagram [40, 42]. On the other hand, calculations based on the quasi-two-dimensional model [110] give highly overestimated results at variance with experimental findings. (Unfortunately, a detailed comparative analysis of the results obtained in Refs [110] and [111] using this model has not been performed thus far.) G Solt [112] tried to calculate the phase diagram for beryllium by expanding the dependence of the cross section area on quasimomentum, $A(k_z)$, with regard not only for the second-order terms (as in the LK formula) but also for the terms of higher orders. The results obtained much better agreed with the experimental data available at that time, as shown in Fig. 31 [112]. In this figure, the experimental findings obtained by the μSR method are compared with the results calculated using the conventional LK formula, the modified formula proposed in Ref. [112], and the quasi-two-dimensional model [110].

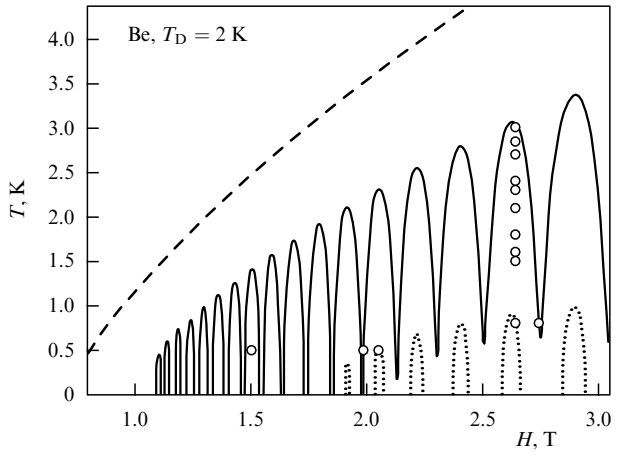

Figure 31. Comparison of experimental data and calculated results using different phase diagram models for beryllium in magnetic fields up to 3 T. Circles display diamagnetic domains experimentally found by the μSR method at different temperatures [42]. Dashed curve (without oscillations) corresponds to the quasi-two-dimensional model [110], solid oscillating curve (beats) to modified formula [112] (in both cases, $T_D = 2$ K), and dotted curves to conventional LK formula assuming $T_D = 1.6$ K (because according to this formula there are no domains whatever at $T_D = 2$ K).

Comparison of Figs 30 and 31 demonstrates that the results of calculations in weak magnetic fields using the modified formula [112] are in satisfactory agreement with the data obtained by the μSR method, and partly, but not completely, agree with the phase diagram. Specifically, the phase boundary for nodes is much higher than in the theory. The most pronounced difference from calculated results is observed, however, in strong magnetic fields. Domains actually disappear much sooner than predicted. We believe that the main contribution to this discrepancy is made by the excess elastic energy of lattice deformation in the domain wall, as mentioned on several occasions in this review (this energy was disregarded in all calculations). Its relative contribution certainly grows with increasing magnetic field. This fact is of special importance for beryllium characterized by anisotropic lattice deformation in the domain wall.

The study of the phase diagram in silver implied agreement with theoretical calculations using the LK formula. Such agreement reported in an earlier work [69] was attributed to the spherical shape of the Fermi surface. Nevertheless, we deemed it worthwhile to measure the phase boundary in silver more thoroughly and over a wider magnetic field range by the newly described method [113].

The study sample was chosen from the same stock as in the experiments with the use of Hall probes, described in Section 3.3. The pickup coil system was also described earlier, with the modulation frequency varying from 20 to 200 Hz. Measurements were made in both a superconducting solenoid with the magnetic field up to 16 T and a resistive magnet with the magnetic field up to 30 T. Such experimental design provided a wide range of overlapping measurements in superconducting and resistive solenoids. The entire coil assembly together with the sample was tilted roughly 13°, so that the dHvA spectrum contained a single cross section with frequency $F = 47{,}300$ T (belly). The temperature was varied between 1.3 and 4.2 K.

The origin of hysteresis had several consequences, each of which can, in principle, be used to determine the point of intersection of the phase boundary. Measurements in strong fields of the resistive magnet may be difficult to make due to intense noise and poor field homogeneity. Therefore, we employed (for comparison) all the methods for the detection of the origin of hysteresis, described in Section 4 and including truncation of the susceptibility amplitude, phase shift (imaginary component), and third-harmonic generation.

Each of these effects was measured separately under identical conditions, i.e., at the same point in the phase plane (T, H). The magnetic field was varied at constant temperature. Each time, we found the appropriate value of the critical field for the transition to the two-phase state and compared the results. Figure 32 illustrates the origin of hysteresis in silver, apparent as the amplitude cutoff effect and a stronger 3rd-harmonic signal.

Figure 32 clearly demonstrates the origin of hysteresis; it shows that both modulation levels, 0.2 and 1.0 G, are significantly smaller than the dHvA period amounting to 20 G in the given field. Due to this, response signal amplitudes are identical in the homogeneous region (see Fig. 32c, e at $H \approx 8$ T). The discrepancy, i.e., 'amplitude truncation', arises at about $H_1 \approx 10$ T. Similarly, the 3rd-harmonic amplitude

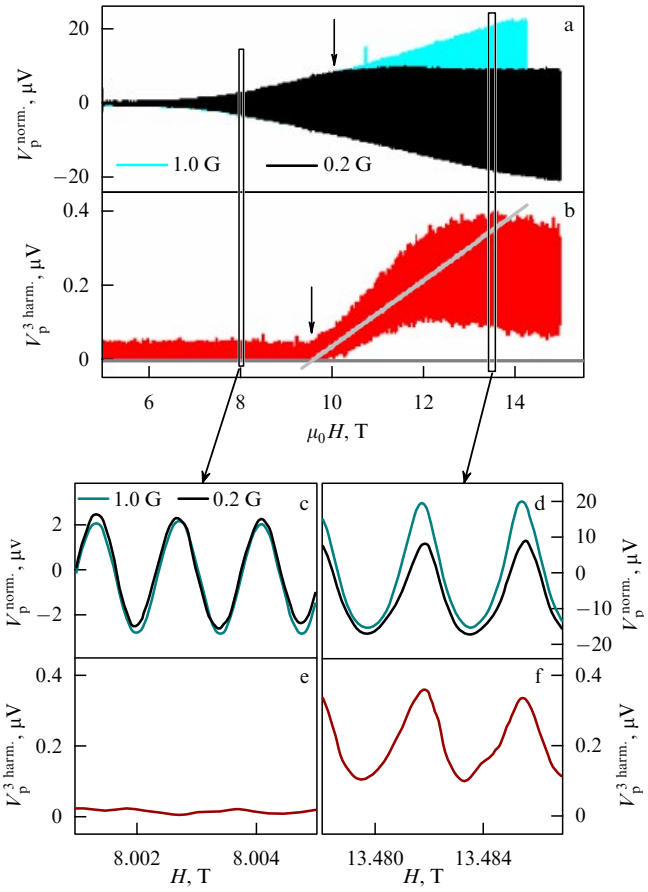

Figure 32. The dHvA effect in silver at 2.7 K and modulation frequency of 160 Hz. (a) Normalized signal amplitude for two modulation levels, 0.2 G (dark-shaded area) and 1.0 G (light-shaded area). The amplitude cutoff effect becomes apparent near $H = 10$ T (arrow). (b) Third harmonic of the pickup voltage measured at 0.2-G modulation amplitude. Abrupt origin of the signal (marked by arrow) happens at $H \approx 9.5$ T. (c, d) Fragments of figure (a) plotted on a larger scale. (e, f) Fragments of figure (b) plotted on a larger scale.

in the field region of about 8 T remains at the noise level, and begins to sharply increase around 10 T (or at $H_2 \approx 9.5$ T, to be precise).

Obviously, the second method has important advantages over the first one, where the correct choice of at least two successive measurement processes with different modulation levels is essential (although it gives a coercive force value). Moreover, the signal-to-noise ratio in the second method is much greater than in the first (measuring the amplitude difference), despite the threshold character of both effects. It is worth noting that the increase in the 3rd-harmonic amplitude is accompanied by the upward shift of the minimal signal level, which must 'ideally' remain zero, as in Fig. 26a. Indeed, the sample remains homogeneous in each dHvA period in the diamagnetic phase, and the 1st-harmonic signal must not exceed the level noise. At least two factors may be responsible for such behavior. First, the inhomogeneity of the magnetic field in the superconducting solenoid (16 T) is three times (30 times in the resistive magnet) greater, whereas the dHvA oscillation period in silver is much smaller (compared with beryllium). Second, the sweep rate in the case being discussed is higher, and still higher in the resistive magnet. Nevertheless, the critical field value remains practically unshifted, despite the aforementioned deviation from the 'ideal' picture, as confirmed in subsequent experiments.

Two more options are feasible: measurement of the phase angle of the 3rd harmonic, and of the imaginary part of the 1st harmonic of the signal. As long as the amplitude of the 3rd harmonic is smaller than the noise level, the phase remains indeterminate and also 'makes noise', from $-\pi$ to $+\pi$. A transition to the two-phase state induces hysteresis and the 3rd harmonic, and the phase angle also becomes determinate. It gives the critical field value $H_3 = 9.8$ T. The appearance of the imaginary part of the 1st harmonic in silver is less noticeable than in beryllium. In the homogeneous state, this signal differs from zero and does not appreciably change with magnetic field variations due to much lower magnetoresistance and, accordingly, eddy currents induced by a variable modulation field in silver. Nevertheless, the response lag changes dramatically with the origin of hysteresis, and the critical field may be taken as $H_4 = 9.3$ T.

All four methods yield very similar estimates of the critical field, from 9.3 to 10 T, in excellent agreement with the results of extrapolation of Hall probe measurements. Therefore, any of these methods can, in principle, be used for the determination of the phase diagrams. But the simplest and most accurate method for silver is the measurement of the 3rd harmonic, as shown by experiments in a resistive magnet.

Measurements in a water-cooled resistive magnet encounter difficulties that are less severe or nonexistent in a superconducting solenoid. Field homogeneity and stability in the magnet are much lower, which accounts for the very high noise level. Both modulation frequency and amplitude had to be increased to maintain the required signal-to-noise ratio. Third-harmonic measurements proved especially insensitive to the change in these parameters, and the critical field value remained practically unshifted in a wide range of modulation frequency and amplitude variations. This observation was verified by measurements in both the superconducting solenoid and the resistive magnet. The results are presented in Fig. 33.

Figure 33 depicts the amplitude of the 3rd harmonic averaged over dHvA oscillations in a wide range of modulation frequency and amplitude variations. A rise in the modulation level to 10.0 G does not shift the critical field value, nor is it affected by a 4-fold change in the modulation

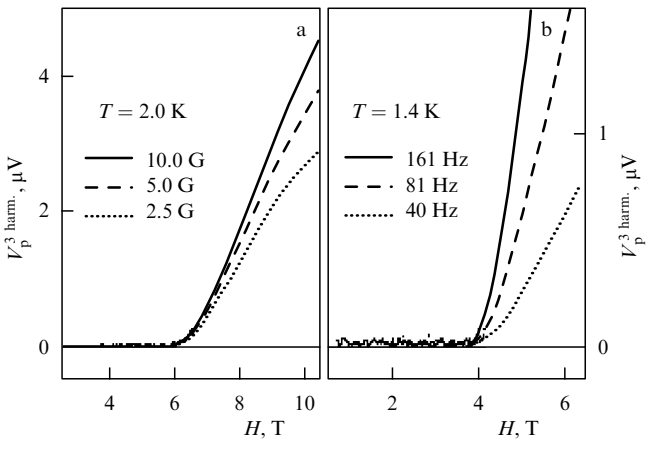

Figure 33. Modulation amplitude (a) and frequency (b) dependences of the 3rd-harmonic amplitude measured in a resistive magnet in silver. Temperatures are indicated in the figure.

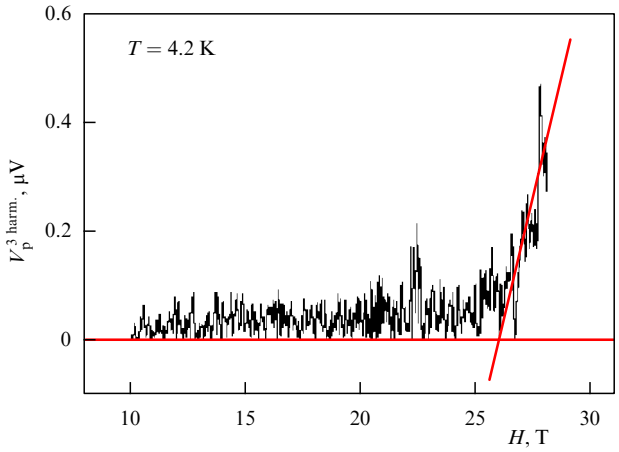

Figure 34. Example of recording 3rd harmonic in a resistive magnet at H up to 28.0 T.

frequency. The results of measurements in the resistive magnet shown in Fig. 33 and those in the superconducting solenoid overlap and coincide. Such stability at varying modulation frequency and amplitude made it possible to find points of the phase diagram for silver at all (even the highest) available magnetic fields. An example of recording the point of transition to the two-phase state near the top of the phase diagram is presented in Fig. 34, clearly demonstrating a rise in the noise level.

The results of all measurements in the superconducting solenoid and the resistive magnet in the plane (H, T) are presented in Fig. 35.

To sum up, the phase diagram for silver, unlike that for beryllium, perfectly matches the phase diagram computed in the framework of the LK approximation. Measurement of the 3rd harmonic proved to be the method of choice for detecting the point of intersection of the phase diagram in metals with high conductivity. For high-resistant metals like beryllium, measurements can be confined to the 1st harmonic, registering its imaginary part in the response signal.

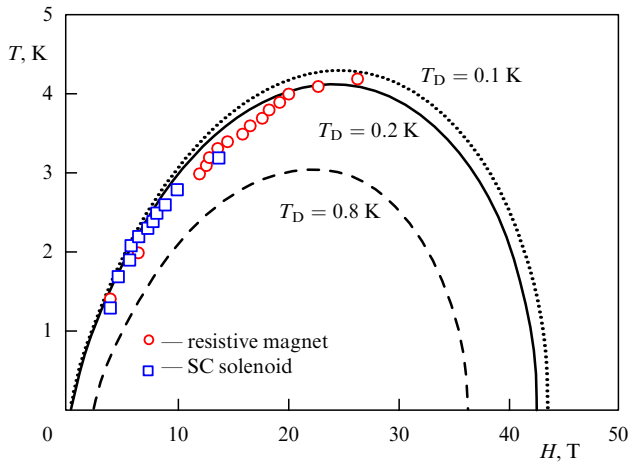

Figure 35. Phase diagrams of the domain state in silver. Dotted, solid, and dashed curves demonstrate the results of calculations by the LK formula at Dingle temperatures 0.1, 0.2, and 0.8 K, respectively. All experimental points obtained both in the superconducting solenoid (squares) and in the resistive magnet (circles) agree well with calculations at $T_D = 0.2$ K.

6. Conclusions

The application of the μSR method for the study of diamagnetic (Condon) domains permitted observing their formation in beryllium, tin, lead, indium, and aluminium, i.e., in all metals investigated thus far. It was shown for the first time (in tin) that domains arise in a perfect crystal at a fairly low temperature, even when the dHvA effect amplitude is much smaller than the period. The formation of Condon domains due to the dHvA effect from two different cross sections of the Fermi surface was also observed for the first time in tin. These data underscore the universal character of the phenomenon. The possibility of reliably recording domain formation from oscillations of $\lambda(H)$ dependence was substantiated and demonstrated in all the cases.

The domain structure on the silver surface was measured for the first time by Hall microprobes. The value of induction inhomogeneity ΔB on the surface was in excellent agreement with that in the bulk, as described by Condon. The transverse dimensions of the domain structure in silver at a magnetic field of 10 T (period $p \geqslant 150$ μm, domain wall thickness $w \sim 20$ μm) proved much greater than predicted ($p \sim 30$ μm, $w \sim 1$ μm) in the theory.

Similar thorough experiments designed to discover diamagnetic domains in beryllium with its 10-times-greater expected amplitude of ΔB failed to reveal their presence. The main conclusion ensuing from our experiments is that Condon domains exist only in the bulk of beryllium. This fact may account for the failure of all preceding beryllium experiments, including those of Condon himself with the use of the NMR technique [14].

We first measured magnetostriction in beryllium during the formation of diamagnetic domains. It was shown that phases with opposite magnetizations correspond to opposite lattice deformation with inverted electron density. Due to this, the charge density gradient in the domain wall creates magnetization current in the magnetic field, which is necessary for the induction difference to arise between the neighboring phases. On the other hand, magnetostriction ensures exact compensation of Fermi level oscillations and there is no contact potential difference between the phases. Such a situation takes place only when metal compressibility is governed entirely by electron gas compressibility.

Lattice deformation in the domain wall produces an excess elastic energy that causes wall thickening; this provides a qualitative explanation for the discrepancy between the data obtained in silver and the results of the Privorotskii theory, and for the absence of a surface domain structure in beryllium in which this deformation is anisotropic.

Hysteresis was revealed in the dHvA effect during transition to the state with diamagnetic domains. Hysteresis in beryllium and silver was estimated at 2 and 0.2 G, respectively. At the same time, the standard modulation method revealed a dramatic change in the response signal and a threshold increase of the 3rd harmonic. In addition, hysteresis was found to account for the Plummer effect which was discovered earlier but had remained unexplained until recently.

The threshold changes in the response signal during the intersection of the phase boundary of the domain state were used to experimentally determine the phase diagram for Condon domains in silver and beryllium. Phase diagrams for domains in silver were constructed in a magnetic field

range up to 28 T, and in beryllium over the entire field range at temperatures of up to 1.3 K. It is ascertained that the results obtained are in excellent agreement with those theoretically predicted for silver but are substantially different from calculations for beryllium, especially in the high magnetic field region.

Acknowledgments. I am grateful to all my coworkers in different countries and institutions. Our joint work not only was fruitful but also provided the pleasure of companionship and mutual understanding. Special thanks are due to L A Maksimov and V P Mineev for enlightening discussions, and to V F Gantmakher and V S Edel'man for the gift of high-quality signal crystals.

7. Appendix. Exact compensation of dia- and paramagnetic currents

Let us consider electron motion along the Larmor orbit of radius R in the plane perpendicular to the magnetic field (Fig. 36). The total diamagnetic moment from all electrons in the 'potential box', i.e., a square with side $a \gg R$, has the form

$$M_- = c^{-1} N a^2 J_0 S_0 \,,$$

where c is the speed of light, N is the surface electron density, $J_0 = \omega e/(2\pi)$ is the electric current of an electron moving in the Larmor orbit, ω is the cyclotron frequency, and $S_0 = \pi R^2$ is the orbit area. As a result, the diamagnetic moment is defined in the following way:

$$M_- = \frac{1}{2c}\, N a^2 \omega e R^2 \,.$$

The compensatory paramagnetic moment is the result of electron motion in the truncated arcs along the square boundary (Fig. 37a).

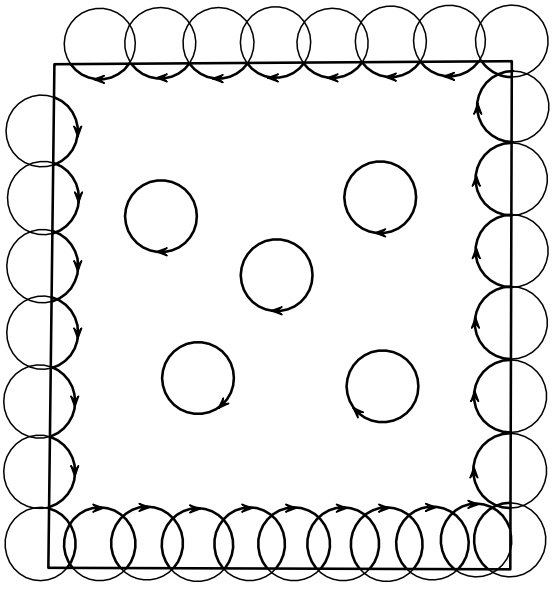

Figure 36. Electron motion along Larmor orbits located entirely inside the square and moving close to the edge. Arrows show the direction of electron rotation (taken from the book by Peierls [73]).

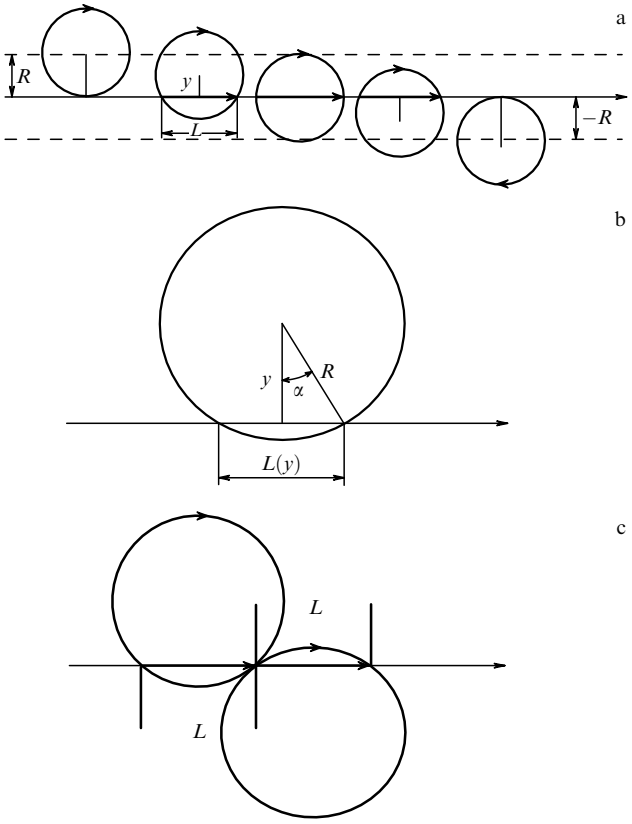

Figure 37. (a) Electron motion in the arcs along the square boundary; y — distance from orbit centers to the sample edge, L — length of a chord over which the charge of an electron moving in the orbit is transferred. (b) Detailed representation of a truncated orbit. (c) Two orbits symmetric with respect to the cutting line, i.e., the sample edge. One has its center inside the sample, and the other outside the sample.

All orbits lying at a distance of $|y| < R$ from the square edge are cut and the arcs remain inside the square. The total number of such arcs (former circumferences) equals

$$n = 4a2RN = 8NaR \,.$$

The mean value $L_{\rm av}$ of displacements $L(y)$ is found by integrating over all arcs:

$$L_{\rm av} = \frac{1}{2R} \int_R^{-R} L(y)\, {\rm d}y \,.$$

Making the substitution of variables in accordance with the detailed representation of an orbit in Fig. 37b: $y = R\cos\alpha$, ${\rm d}y = -R\sin\alpha\, {\rm d}\alpha$, $L(y) = 2R\sin\alpha$, we have

$$L_{\rm av} = \frac{1}{2R} \int_0^{\pi} 2R^2 \sin^2\alpha\, {\rm d}\alpha = R \int_0^{\pi} \sin^2\alpha\, {\rm d}\alpha \,.$$

On the interval $(0, \pi)$, one finds

$$\int_0^{\pi} \sin^2\alpha\, {\rm d}\alpha \equiv \int_0^{\pi} \cos^2\alpha\, {\rm d}\alpha \,;$$

whence it follows that

$$L_{\rm av} = \frac{\pi R}{2} \,.$$

Let us find now the mean velocity $v_{\rm av}$ of electron motion along the sample boundary. To this effect, we shall simultaneously consider two symmetric orbits defined by angles α and $2\pi - \alpha$ (Fig. 37c). The same chord length L corresponds to either orbit, and the total time of electron motion along such conjugate symmetric orbits is equal to the period $T = 2\pi/\omega$. The totality of electrons can be broken down into matched pairs such that the velocity of electrons in the orbits $v = 2L/T$ and, accordingly, the mean velocity of electron motion along the boundary is given by

$$v_{\rm av} = \frac{2L_{\rm av}}{T} = \frac{\omega R}{2} .$$

Thus, the electron makes a complete turn around the sample for a mean time

$$t^* = \frac{4a}{v_{\rm av}} = \frac{8a}{\omega R} .$$

The current created by the motion of one electron is defined as

$$\frac{e}{t^*} = \frac{e\omega R}{8a} .$$

Multiplying the last quantity by the number of electrons in the jumping orbits, we arrive at the total current and the value of the magnetic moment. To recall, the total number of orbits cut by the square edge is n, and each orbit was occupied by one electron before it was cut. Because the number of electrons is very high and they are equiprobably distributed over the orbit circumference, they are equally likely to find themselves inside or outside the sample-square. In other words, exactly half of the electrons remained outside the sample. This means that the number of electrons hopping along the boundary and generating paramagnetic current is $n/2$. Hence, for paramagnetic current and, accordingly, for the magnetic moment one finds the following expressions

$$J_+ = \frac{ne}{2t^*} = \frac{1}{2} Ne\omega R^2 ,$$
$$M_+ = \frac{1}{2c} Na^2 e\omega R^2 ,$$

i.e., one has

$$M_+ = M_- ,$$

which was to be proved.

References

1. Condon J H *Phys. Rev.* **145** 526 (1966)
2. Landau L *Z. Phys.* **64** 629 (1930); Landau L *Sobranie Trudov* Vol. 1 (Collected Works) (Moscow: Nauka, 1969) p. 47
3. de Haas W J, van Alphen P M *Proc. Netherlands R. Acad. Sci. Amsterdam* **33** 1106 (1930)
4. Lifshits I M, Azbel' M Ya, Kaganov M I *Zh. Eksp. Teor. Fiz.* **31** 63 (1956) [*Sov. Phys. JETP* **4** 41 (1957)]
5. Lifshits I M, Peschanskii V G *Zh. Eksp. Teor. Fiz.* **35** 1251 (1958) [*Sov. Phys. JETP* **8** 875 (1959)]
6. Onsager L *Philos. Mag.* **43** 1006 (1952)
7. Lifshits I M, Kosevich A M *Zh. Eksp. Teor. Fiz.* **29** 730 (1955) [*Sov. Phys. JETP* **2** 636 (1956)]
8. Shoenberg D *Magnetic Oscillations in Metals* (Cambridge: Cambridge Univ. Press, 1984) [Translated into Russian (Moscow: Mir, 1986)]
9. Pippard A B *Proc. R. Soc. London A* **272** 192 (1963)
10. Egorov V S *HAIT J. Sci. Eng.* **1** 647 (2004)
11. Abrikosov A A *Osnovy Teorii Metallov* (Fundamentals of the Theory of Metals) (Moscow: Nauka, 1987) [Translated into English (Amsterdam: North-Holland, 1988)]
12. Privorotskii I A *Zh. Eksp. Teor. Fiz.* **52** 1755 (1967) [*Sov. Phys. JETP* **25** 1167 (1967)]
13. Privorotskii I *Thermodynamic Theory of Domain Structures* (New York: Wiley, 1976)
14. Condon J H, Walstedt R E *Phys. Rev. Lett.* **21** 612 (1968)
15. Alekseevskii N E, Slutskin A A, Egorov V S *J. Low Temp. Phys.* **5** 377 (1971)
16. Egorov V S *Zh. Eksp. Teor. Fiz.* **69** 2231 (1975) [*Sov. Phys. JETP* **42** 1135 (1975)]
17. Egorov V S *Zh. Eksp. Teor. Fiz.* **72** 2210 (1977) [*Sov. Phys. JETP* **45** 1161 (1977)]
18. Bozhko V I, Vol'skii E P *Pis'ma Zh. Eksp. Teor. Fiz.* **26** 337 (1977) [*JETP Lett.* **26** 223 (1977)]
19. Vol'skii E P *Pis'ma Zh. Eksp. Teor. Fiz.* **26** 585 (1977) [*JETP Lett.* **26** 437 (1977)]
20. Markiewicz R S, Meskoob M, Zahopoulos C *Phys. Rev. Lett.* **54** 1436 (1985)
21. Smith J L, Lashley J C *J. Low Temp. Phys.* **135** 161 (2004)
22. Markiewicz R S *Phys. Rev. B* **34** 4172 (1986)
23. Markiewicz R S *Phys. Rev. B* **34** 4177 (1986)
24. Markiewicz R S *Phys. Rev. B* **34** 4183 (1986)
25. Gordon A, Vagner I D *J. Phys. Condens. Matter* **2** 3687 (1990)
26. Gordon A et al. *Phys. Lett. A* **160** 315 (1991)
27. Gordon A et al. *Phys. Rev. B* **43** 3775 (1991)
28. Gordon A, Vagner I D, Wyder P *Solid State Commun.* **87** 1155 (1993)
29. Lifshits I M *Zh. Eksp. Teor. Fiz.* **38** 1569 (1960) [*Sov. Phys. JETP* **11** 1130 (1960)]
30. Varlamov A A, Egorov V S, Pantsulaya A V *Adv. Phys.* **38** 469 (1989)
31. Blanter Ya M, Kaganov M I, Posvyanskii D V *Usp. Fiz. Nauk* **165** 213 (1995) [*Phys. Usp.* **38** 203 (1995)]
32. Schenck A *Muon Spin Rotation Spectroscopy* (Bristol: A. Hilger, 1986)
33. Belousov Yu M, Smilga V P *Fiz. Tverd. Tela* **21** 2459 (1979) [*Sov. Phys. Solid State* **21** 1416 (1979)]
34. Belousov Y M, Smilga V P, in *Proc. 3rd Intern. Symp. on Muon and Pion Interaction with Matter, JINR, Dubna, 1995*
35. Solt G et al. *Phys. Rev. Lett.* **76** 2575 (1996)
36. Solt G, Egorov V S *Physica B* **318** 231 (2002)
37. Solt G et al., in *9th Intern. Conf. μSR-2002, N-38, Williamsburg, USA, 2002*
38. Lykov F V, in *Trudy Mezhdunar. Konf. po Fizike Nizkikh Temperatur NT-32* (Proc. of the Intern. Conf. on Low Temperature Physics) (Kazan': Kheter, 2000) p. 76
39. Tripp J H et al. *Phys. Rev.* **180** 669 (1969)
40. Egorov V S *Fiz. Tverd. Tela* **30** 1253 (1988)
41. Osborn J A *Phys. Rev.* **67** 351 (1945)
42. Solt G et al. *Phys. Rev. B* **59** 6834 (1999)
43. Solt G et al. *Hyperfine Interact.* **104** 257 (1997)
44. Pudalov V M, in *Elektrony Provodimosti* (Conduction Electrons) (Eds M I Kaganov, V S Edel'man) (Moscow: Nauka, 1985) p. 416
45. Craven J E *Phys. Rev.* **182** 693 (1969)
46. Gantmakher V F *Zh. Eksp. Teor. Fiz.* **44** 811 (1963) [*Sov. Phys. JETP* **17** 549 (1963)]
47. Gantmakher V F *Zh. Eksp. Teor. Fiz.* **46** 2028 (1964) [*Sov. Phys. JETP* **19** 1366 (1964)]
48. Pudalov V M, Khaikin M S *Zh. Eksp. Teor. Fiz.* **67** 2260 (1974) [*Sov. Phys. JETP* **40** 1121 (1974)]
49. Stafleu M D, de Vroomen A R *Phys. Status Solidi B* **23** 676 (1967)
50. Stafleu M D, de Vroomen A R *Phys. Status Solidi B* **23** 683 (1967)
51. Roger W A, Woods S B *J. Phys. F* **6** 2289 (1976)
52. Vaughan R W, Elleman D D, McDonald D G *J. Phys. Chem. Solids* **31** 117 (1970)
53. Deacon J M, Mackinnon L *J. Phys. F* **3** 2082 (1973)
54. Gantmakher V F, Private communication
55. Larson C O, Gordon W L *Phys. Rev.* **156** 703 (1967)
56. Anderson J R, O'Sullivan W J, Schirber J E *Phys. Rev. B* **5** 4683 (1972)
57. Anderson J R, Lee J Y M, Stone D R *Phys. Rev. B* **11** 1308 (1975)

58. Landau L D *Zh. Eksp. Teor. Fiz.* **7** 371 (1937); Landau L *Phys. Z. Sowjetunion* **11** 129 (1937)
59. Livingstone J D, de Sorbo W, in *Superconductivity* Vol. 2 (Ed. R D Parks) (New York: M. Dekker, 1969) p. 1235
60. Sharvin Yu V *Zh. Eksp. Teor. Fiz.* **33** 1341 (1958) [*Sov. Phys. JETP* **6** 1031 (1958)]
61. Egorov V S et al., in *9th Intern. Conf. μSR-2002, Williamsburg, USA, 2002*
62. Egorov V S et al. *Phys. Rev. B* **64** 024524 (2001)
63. Meshkovskii A G, Shal'nikov A I *Zh. Eksp. Teor. Fiz.* **17** 851 (1947)
64. Pugel E et al. *Appl. Phys. Lett.* **71** 2205 (1997)
65. Simpkins J E *Rev. Sci. Instrum.* **39** 570 (1968)
66. Gasparov V A *Zh. Eksp. Teor. Fiz.* **68** 2259 (1975) [*Sov. Phys. JETP* **41** 1129 (1975)]
67. Gasparov V A, Huguenin R *Adv. Phys.* **42** 393 (1993)
68. Zernov V B, Sharvin Yu V *Zh. Eksp. Teor. Fiz.* **36** 1038 (1959) [*Sov. Phys. JETP* **9** 737 (1959)]
69. Kramer R B G et al. *Physica B* **362** 50 (2005)
70. Joseph A S, Thorsen A C *Phys. Rev.* **138** A1159 (1965)
71. Gordon A, Itskovsky M A, Wyder P *Phys. Rev. B* **59** 10864 (1999)
72. Kramer R B G et al. *Phys. Rev. Lett.* **95** 267209 (2005)
73. Peierls R *Surprises in Theoretical Physics* (Princeton, NJ: Princeton Univ. Press, 1979) [Translated into Russian (Moscow: Nauka, 1988)]
74. van Leuven J A *J. Physique* **2** 361 (1921)
75. Vagner I D, Private communication
76. Teller E *Z. Phys.* **67** 311 (1931)
77. Bloch F "Molekulartheorie des Magnetismus", in *Handbuch der Radiologie* Vol. 2 (Leipzig: Akad. Verlagsgesellschaft, 1934) [Translated into Russian (Leningrad–Moscow: ONTI, 1936)]
78. Mineev V P *Phys. Rev. B* **75** 193309 (2007)
79. Mineev V P *Phys. Rev. B* **76** 209902(E) (2007)
80. Frank-Kamenetskii D A *Lektsii po Fizike Plazmy* (Lectures on Plasma Physics) (Moscow: Atomizdat, 1968)
81. Egorov V S *Fiz. Tverd. Tela* **32** 684 (1990)
82. Egorov V S, Lykov Ph V *Zh. Eksp. Teor. Fiz.* **121** 191 (2002) [*JETP* **94** 162 (2002)]
83. Egorov V S, Lykov F V, Repina O A *Pis'ma Zh. Eksp. Teor. Fiz.* **72** 28 (2000) [*JETP Lett.* **72** 18 (2000)]
84. Kapitza P *Proc. R. Soc. London A* **135** 568 (1932)
85. Chandrasekhar B S *Phys. Lett.* **6** 27 (1963)
86. Thompson T E et al. *Phys. Rev. B* **4** 518 (1971)
87. Chandrasekhar B S et al., in *Proc. of LT10, VINITI, Moscow* Vol. 3 (1967) p. 328
88. White G K *Cryogenics* **1** 151 (1961)
89. Smith J F, Arbogast C L *J. Appl. Phys.* **31** 99 (1960)
90. Grigoriev I S, Meilikhov E Z (Eds.) *Fizicheskie Velichiny*: *Spravochnik* (Handbook of Physical Quantities) (Moscow: Energoatomizdat, 1991) [Translated into English (Boca Raton, NY: CRC Press, 1996)]
91. Faber T E *Proc. R. Soc. London A* **248** 460 (1958)
92. Loucks T L, Cutler P H *Phys. Rev.* **133** A819 (1964)
93. Terrell J H *Phys. Rev.* **149** 526 (1966)
94. Watts B R *Proc. R. Soc. London A* **282** 521 (1964)
95. Lazarev B G, Kaner E A, Chebotarev L V *Fiz. Nizk. Temp.* **3** 808 (1977) [*Sov. J. Low Temp. Phys.* **3** 394 (1977)]
96. Ashkenazi J et al. *Phys. Rev. B* **18** 4120 (1978)
97. Kaganov M I, Lifshits I M, Sinel'nikov K D *Zh. Eksp. Teor. Fiz.* **32** 605 (1957) [*Sov. Phys. JETP* **5** 500 (1957)]
98. Alekseevskii N E, Nizhankovskii V I *Zh. Eksp. Teor. Fiz.* **88** 1771 (1985) [*Sov. Phys. JETP* **61** 1051 (1985)]
99. Brovman E G, Kagan Yu M *Usp. Fiz. Nauk* **112** 369 (1974) [*Sov. Phys. Usp.* **17** 125 (1974)]
100. du Trémolet de Lacheisserie E, Gignoux D, Schlenker M (Eds) *Magnetism* (Norwell, Mass.: Kluwer Acad. Publ., 2002)
101. Gordon A, Vagner I D, Wyder P *Adv. Phys.* **52** 385 (2003)
102. Kramer R B G et al. *Phys. Rev. Lett.* **95** 187204 (2005)
103. Egorov V S, Preprint IAE-2754 (Moscow: IAE, 1976)
104. Plummer R D, Gordon W L *Phys. Rev. Lett.* **13** 432 (1964)
105. Knecht B et al. *J. Low Temp. Phys.* **29** 499 (1977)
106. Plummer R D, Gordon W L *Phys. Lett.* **20** 612 (1966)
107. Rüdt C et al. *Phys. Rev. B* **69** 014419 (2004)
108. Gordon A, Logoboy N, Joss W *Phys. Rev. B* **69** 174417 (2004)
109. Kramer R B G, Egorov V S, Jansen A G M, Joss W, arXiv.1005.2047
110. Gordon A et al. *Phys. Rev. Lett.* **81** 2787 (1998)
111. Champel T, Mineev V P *Philos. Mag. B* **81** 55 (2001)
112. Solt G *Solid State Commun.* **118** 231 (2001)
113. Kramer R B G, Egorov V S, Gasparov V A, Jansen A G M, Joss W, arXiv.1003.4822